Refining the Moho across the Australian continent

B.L.N. Kennett (1∗), A. Gorbatov (2), H. Yuan (3,4), S. Agrawal (1),
R. Murdie (4), M.P. Doublier (2), C.M. Eakin (1), M.S. Miller (1), L. Zhao (5),
K. Czarnota (2), J.P. O'Donnell (6), M. Dentith (3), K. Gessner (4).

(1) *Research School of Earth Sciences, The Australian National University, Canberra ACT 2601, Australia*
(2) *Geoscience Australia, GPO Box 389, Canberra ACT 2600*
(3) *University of Western Australia*
(4) *Geological Survey of Western Australia*
(5) *Institute of Geology & Geophysics, Chinese Academy of Sciences*
(6) *Geological Survey of South Australia (now at Geological Survey of Western Australia)*

Corresponding author: Brian.Kennett@anu.edu.au

Peer reviewed preprint submitted to EarthArXiv

Accepted for publication in : *Geophysical Journal International*
2023 January 25

doi: 10.193/gji/ggad35

accepted for *Geophys. J. Int.*

Refining the Moho across the Australian continent

B.L.N. Kennett[1+], A. Gorbatov[2], H. Yuan[3,4], S. Agrawal[1], R. Murdie[4], M.P. Doublier[2], C.M. Eakin[1], M.S. Miller[1], L. Zhao[5], K. Czarnota[2], J.P. O'Donnell[6], M. Dentith[3], K. Gessner[4].

[1] *Research School of Earth Sciences, The Australian National University, Canberra ACT 2601, Australia*

[2] *Geoscience Australia, GPO Box 389, Canberra ACT 2600*

[3] *University of Western Australia*

[4] *Geological Survey of Western Australia*

[5] *Institute of Geology & Geophysics, Chinese Academy of Sciences*

[6] *Geological Survey of South Australia**

[+] *Corresponding author: Brian.Kennett@anu.edu.au*

SUMMARY

In recent years there has been a considerable expansion of deployments of portable seismic stations across Australia, which have been analysed by receiver function or autocorrelation methods to extract estimates of Moho depth. An ongoing program of full-crustal reflection profiles has now provided more than 25,000 km of reflection transects that have been interpreted for Moho structure. The Moho dataset is further augmented by extensive marine reflection results. These new data sources have been combined with earlier refraction and receiver function results to provide full continental coverage, though some desert areas remain with limited sampling.

The dense sampling of the Moho indicates the presence of rapid changes in Moho depth and so the Moho surface has been constructed using an approach that allows different weighting and spatial influence depending on the nature of the estimate. The inclusion of

Moho results from continental-wide gravity inversion with low weighting helps to resolve the continent-ocean transition and to provide additional control in the least sampled zones. The refined distribution indicates the presence of widespread smaller-scale variations in Moho structure. Strong lateral contrasts in crustal thickness remain, but some have become more subdued with improved sampling of critical areas. The main differences from earlier results lie in previously poorly sampled regions around the Lake Eyre Basin, where additional passive seismic results indicate somewhat thicker crust though still with a strong contrast in crustal thickness to the cratonic zone to the west.

Key words: Crustal Structure; Controlled source seismology; Body waves; Australia;

1 INTRODUCTION

From the original identification of the base of the crust by Mohorovičić (1910) until the 1980's the principal means of determining the depth to the Moho came from seismic refraction observations. However, more recently a range of receiver-based techniques exploiting distant earthquakes have provided additional information. In Australia, the use of receiver functions exploiting P to S conversions was pioneered by Shibutani et al. (1996) using waveform inversion. The first continent-wide study was made by Clitheroe et al. (2000) exploiting the portable stations deployed in the SKIPPY experiment (van der Hilst et al. 1994). Subsequently both waveform inversion procedures and stacking methods have been employed with extensive deployments of portable stations (e.g., Reading et al. 2003, 2007, 2011, Yuan 2015, Sippl et al. 2017). Correlation techniques have also proved to be valuable. Gorbatov et al. (2013) showed how autocorrelation of continuous records could recover the reflection response for P waves beneath a station. This approach was applied across a broad swath of stations in southeastern Australia by Kennett et al. (2015), with stacking of nearby stations to enhance the stability of the results. The same portion of the seismic record for teleseisms as used with conventional receiver functions can be used directly with autocorrelation (Sun & Kennett 2016, Qashqai et al. 2019, Liang & Kennett 2020). This approach has advantages in regions with complex near-surface structures where reverberations obscure the receiver function response (e.g., Kennett & Liang 2021).

The coverage of Australia with seismic stations has grown from just a few permanent seismic stations to a much enhanced national network (Geoscience Australia, 2021) augmented by stations

⋆ now at Geological Survey of Western Australia

from the Australian Seismometers in Schools project AuSIS (Balfour et al. 2014). Deployments of broad-band portable stations starting in the 1990's have now covered much of the continent. Investment from the Australian National University, Australian Research Council grants and the AuScope infrastructure program has seen dense coverage in central and eastern Australia. The *Exploring for the Future* program from Geoscience Australia has dramatically increased coverage in northern Australia. In western Australia a number of deployments have been supported in part by the Geological Survey of Western Australia with additional input from the Institute of Geology & Geophysics, Chinese Academy of Sciences (IGGCAS). The net result is there is now good continental coverage of Moho estimates (Figure 1), though the density of stations is somewhat variable. In desert regions results are largely confined to limited transport access corridors.

The large-scale program in passive seismology in Australia has been complemented by continuing full-crustal reflection profiling that now provides over 25,000 km of coverage with transects spanning the full width of the continent. Such reflection profiles have revealed the complex crustal architecture of Australia from the Precambrian cratons in the west and centre to the Phanerozoic fold belts in the east (e.g., Korsch & Doublier 2015), as well as detail of variations in the Moho (Figure 1).

With many different styles of estimates of the depth to the Moho the issue of a suitable approach for exploiting all the available information becomes important. A smooth Moho surface can be sought, and this is the approach used by Kennett et al. (2011) and Salmon et al. (2013). Averaged estimates of Moho depth were assigned to the centre of 0.5 degree cells and a tensioned spline interpolation (Smith & Wessel, 1990) was employed to provide a continent-wide surface as in Figure 2. The variability of the Moho estimates within the cells provides an indicator of the reliability of the results. Such a procedure cannot include sharp jumps in Moho depth, revealed particularly in reflection profiling, nor readily accommodate very uneven sampling. An alternative approach developed by Kennett (2019) is to assign a weight and Gaussian influence zone around each data point, and employ the full data set to extract Moho estimates on a regular grid (e.g., 0.25 degree) along with a measure of reliability. The updated Moho maps in Section 3 are produced with this approach from the point distribution displayed in Figure 1.

2 PRIOR STUDIES

The first compilation of the Australian Moho from refraction experiments was made by Collins (1991). These results were later augmented with the receiver function estimates of Moho depth from Clitheroe et al. (2000) to produce a continent-wide Moho distribution (Collins et al. 2003). This Moho surface is illustrated in the upper panel of Figure 2, with the control points superimposed using the same colour scheme.

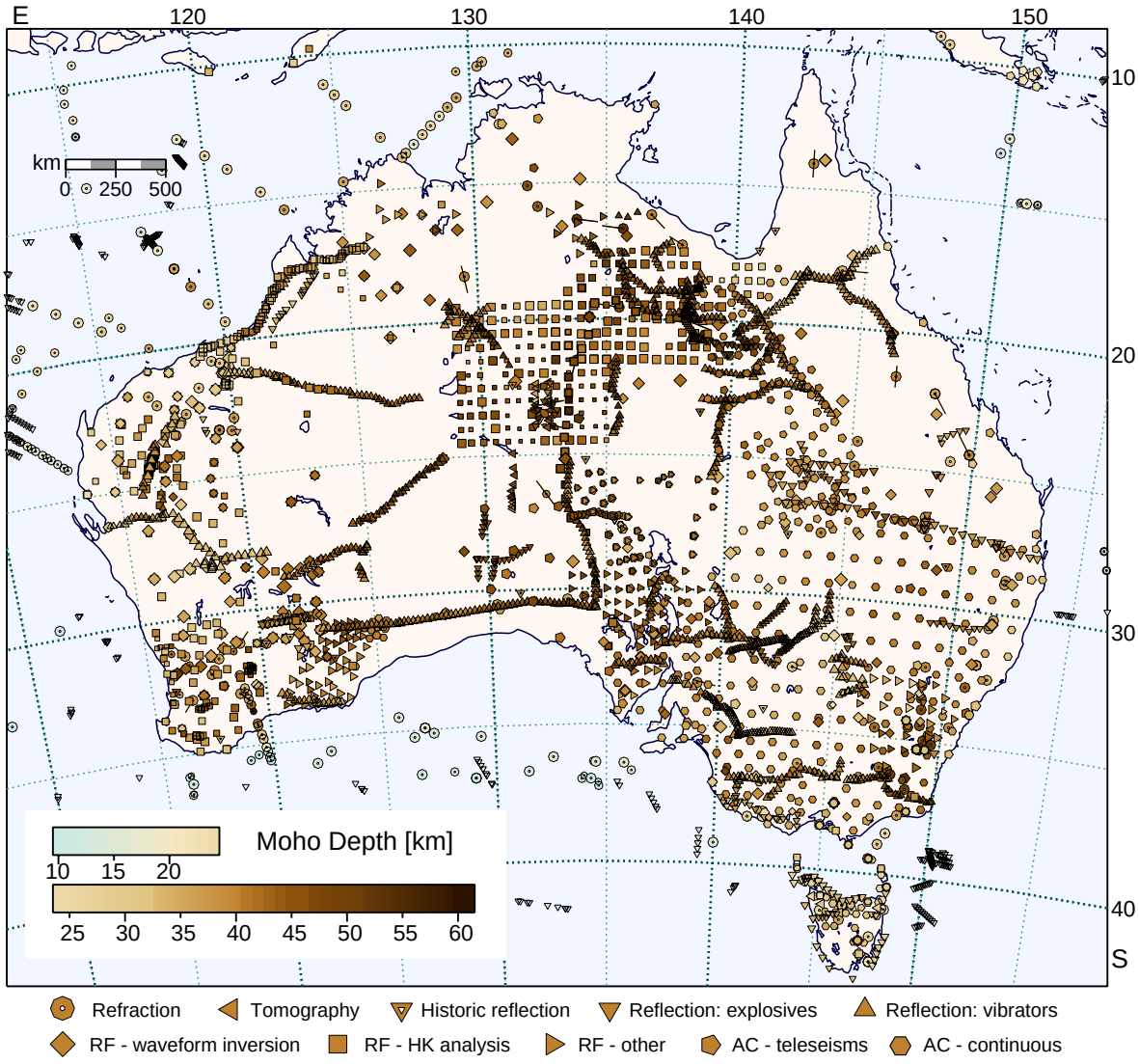

Figure 1. Current Moho estimates across Australia and its surroundings. The 4300 points are organised by style of estimate with a distinctive symbol whose size indicates reliability.

As part of the development of the seismological reference model for Australia (AuSREM), Kennett et al. (2011) put together the full set of available receiver functions, onshore and offshore refraction results, and interpreted Moho from seismic reflection. Some additional reflection profiling in hitherto poorly sampled areas of Western Australia was carried out in 2012, and Salmon et al. (2013) exploited the additional information to produce the Moho surface displayed in the lower panel of Figure 2. Both of the Moho surfaces shown in Figure 2 have been constructed using the same tensioned spline approach. This mode of construction was used up to 2017, when an updated surface incorporating further receiver function stations and reflection work (including marine) was published as Figure 7.16 of Kennett et al. (2018). An alternative approach to Moho surface construction was

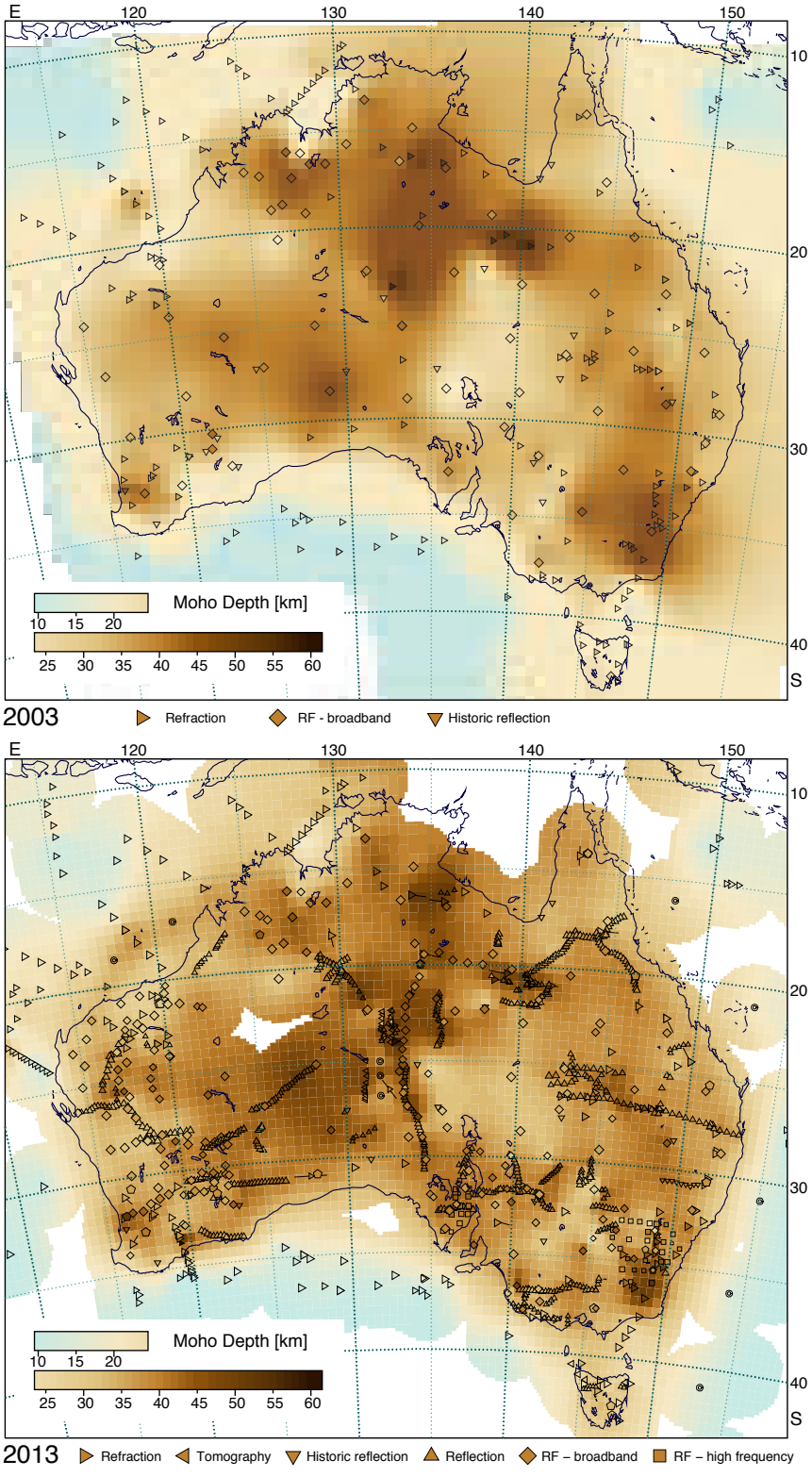

Figure 2. Prior Moho surface results with data points superimposed using the same colour scheme. Upper panel using the 110 Moho depths employed by Collins et al. (2003). Lower panel with the 1380 Moho depths used by Salmon et al. (2013); white areas are inadequately sampled. Both surfaces have been constructed in the same way with tensioned splines, and are represented with 0.5 degree pixels (Wessel & Smith 1998)

explored by Bodin et al. (2012) using a Bayesian probabilistic approach. These ensemble results give a good correspondence for the major features of the Moho surface, but also allow investigation of the local reliability including the possible presence of localised jumps.

3 MOHO MODEL

The latest version of the Moho distribution across the Australian continent draws on a wide range of different classes of information with variable density depending on location. The number of sample points has tripled since the Salmon et al. (2013) compilation to more than 4000. There has been a significant increase in information in Western Australia and in northern central Australia, but still a number of regions remain under sampled. In the desert areas complex logistics has mostly confined information to transects along the few access roads. Land access limitations have also reduced coverage in the northernmost part of Australia.

3.1 Data sets

The cumulative datasets on Moho structure in Australia have involved input from many different institutions. The current distribution of seismic stations across the continent, both permanent and temporary, is illustrated in Figure S1 of the Supplementary Materials with identification of the different contributions. The extensive program of full-crustal reflection profiling across the continent has been led by Geoscience Australia with contributions from the State Geological Surveys and the AuScope infrastructure program. The different classes of data employed are illustrated separately in Figures S2–S4 of the Supplementary Material.

In the earlier Moho compilations refraction data were used as point observations. This was appropriate when the data set was sparse (Collins et al. 2003), but as other data sets have provided much closer spatial sampling it is desirable to make a better representation of the nature of refraction sampling. Figure S2 in the Supplementary Materials displays the distribution of the shot points and recording stations employed in the refraction work together with the control points employed in current analysis. A refraction estimate involves sampling over a distance of about 100 km and to account for the directional nature of the sampling we have split those data points with directional indicators into two separated values with reduced weight.

Most of the new contributions to the receiver function results have been analysed with variants of the H-k stacking approach of Zhu & Kanamori (2000), which is oriented toward a sharp Moho interface. In a number of parts of Australia there is a gradient zone at the base of the crust and so the amplitude of the "Moho" conversion is diminished, which reduces the effectiveness of the stacking

procedure. Nevertheless, with care, good results can be achieved using teleseismic P waves (Yuan 2015, Sippl 2016, Sippl et al. 2017, Gorbatov et al. 2020b). At a few additional sites in southeastern Australia and Tasmania waveform inversion of the receiver functions has been used (Bello et al. 2021).

Estimates of the P wave reflectivity beneath a station can be extracted from continuous seismic records (Gorbatov et al. 2013) or from the same portion of teleseismic P arrivals as used for receiver function studies (Sun & Kennett 2016). These approaches have significantly added to data coverage and resolved some data anomalies. For example, in the south of the Yilgarn Craton there is material with high P wavespeeds but distinctly crustal character. The top of this zone was previously picked, but the autocorrelograms display a second reflector at around 40 km depth that should be identified as the Moho. Because just the vertical component is needed for autocorrelation analysis, it has proved possible to exploit older portable stations in Victoria and South Australia with single component recording. The base of the crust is marked by a sharp decrease in the amplitude of reflectors and lower spatial frequency in depth. For continuous records, the clarity of the crust-mantle transition can be enhanced by spatial stacking, as used by Kennett et al. (2015) for the full suite of portable stations in southeastern Australia.

With closely spaced stations it is possible to obtain direct images of the variations in the lithosphere (Liang & Kennett 2020) and extract Moho information combining receiver function and autocorrelation results. In areas with complex near-surface structure or substantial sediment cover, near-surface S reverberations in receiver functions can extend over the expected time for the Moho conversion hampering identification of the Moho peak. Fortunately, the autocorrelation process works well for such stations and so it is possible to track the Moho across multiple stations as in the work of Kennett & Liang (2021) in the transition from the Thomson Orogen to the Mt. Isa block. Autocorrelation has been used for temporary stations in South Australia and the Mt. Isa region and for a few other stations where Ps receiver functions could not be readily interpreted due to complex near-surface structure, e.g., the permanent station FORT on the Nullabor Plain.

Reflection seismic sounding of the full crust has expanded substantially from the coverage in 2013, and now transects can be extended across the entire continent from east to west. The profiling provides cover for a number of areas with little previous information. The entire set of reflection profiles have been reviewed with Moho picks made, as far as possible, at regular intervals along each profile. Moho estimates from more than 25,000 km of reflection profile are included in the current compilation. Sedimentary corrections have been introduced using information from the shallow parts of the reflection profiles. Efforts have been made to tie the reflection results to portable seismic stations in the vicinity of the profiles. The receiver function Moho estimates from these stations are very valuable for calibration of the conversion from two-way reflection time to depth, but need to be

assessed in the light of the crustal architecture. Sometimes the most prominent discontinuity picked up by the receiver-function approach does not coincide with the base of the reflectivity associated with the crust, but rather the top of a band of reflections at the base of the crust (Kennett & Saygin 2015).

In addition to the onshore reflection results we have added a large number of Moho estimates from marine seismic reflection analysed by Czarnota et al. (2013). These tightly sampled profiles supplement sparser offshore refraction constraints and provide a valuable extension of data coverage into the oceanic domain.

In order to maintain continuity with the earlier studies we concentrate here on the use of receiver function results from passive seismic recordings. However, for stations with no other form of analysis (e.g., stations in the AuSIS network) we have included Moho estimates from waveform inversion of the autocorrelation of teleseismic P waves (Qashqai et al., 2019). We have taken the Moho to lie at the base of any gradient zone from crust to mantle, again maintaining continuity with the results displayed in Figure 2.

As in the work of Kennett et al. (2011) and Salmon et al. (2013), we include tomographic results to improve resolution in critical areas. Linear profiles of portable instruments across the major gravity anomalies in central Australia (Lambeck et al. 1988, McQueen & Lambeck 1996) provide good control on relative crustal variations, with calibration from nearby reflection seismic results. Rawlinson et al. (2010) have developed a model of the crust–mantle boundary in Tasmania from tomography combining refraction results from a marine survey recorded at land stations with teleseismic data recorded at dense seismic arrays.

3.1.1 Exploring for the Future – Geoscience Australia

The importance of a national approach to seismic imaging was highlighted by the UNCOVER initiative (AMIRA 2017). Geoscience Australia (GA) adopted such seismic acquisition as part of the Council of Australian Governments's National Mineral Exploration Strategy (COAG 2017). GA, in collaboration with Australian State and Territory Geological Surveys, academia and AuScope, has expanded the AusArray project to the national scale with the *Exploring For The Future* program (EFTF). The EFTF investment has enabled the unification of available datasets across Australia, and has lead to a doubling of the national rate of new data acquisition. Extensive quality control checks have been applied across the AusArray dataset to improve the robustness of subsequent analysis and interpretation. The final objective is a standardised and quality controlled national half-degree data coverage (Gorbatov et al. 2020a).

Two types of seismic stations are operated by the EFTF program: a movable array with around 150 seismic stations and set of a dozen semi-permanent stations. In each case three-component

broadband seismic sensors are used with a lower corner period of 120 sec. The movable array has been deployed for one year at a time in Northern Australia before it is moved to a new area; whereas the semi-permanent stations operate at fixed positions for the duration of the EFTF program.

All the data collected have had thorough quality checking. Receiver function analysis was performed using H-k stacking following the Chen et al. (2010) variation of the Zhu & Kanamori (2000) approach (Gorbatov et al. 2020b).

3.1.2 Western Australia

Since the release of the AuSREM 2013 model (Kennett et al. 2011, Salmon et al. 2013), there has been a large increase in both portable and permanent station coverage in Western Australia supported by collaboration between academia, industry, and the state government. New data sources and experiments contributing to the current Moho compilation include the following: ALFREX, a 70-station deployment in the east Albany-Fraser Orogen along the southeastern margin of the Yilgarn Craton (Sippl et al. 2017); COPA, a 86-station deployment in the Capricorn Orogen between the Pilbara and Yilgarn Cratons (Yuan et al. 2017); HPS, a 29-station high-density passive-source deployment across the boundary of the Pilbara Craton and Gascoyne Province in the Capricorn Orogen (Dentith et al. 2018, Yuan & Bodin 2018); PBS, a 36-station Perth Basin Passive (PBS) deployment in the Perth Basin (Murdie et al. 2020a); CWAS, a 60-station China-Western Australia Seismic experiment across the onshore northern Canning Basin (Zhao et al. 2022); SWAN, a 27-station enhanced South Western Australia (seismic) Network in the Southwest Terrane of Western Australia (Murdie et al. 2020b, Miller et al. 2023); EGF, a dense set of 22 stations along a 200 km segment of the full-crustal reflection profile to the north of Kalgoorlie in the Eastern Goldfields (Tian et al. 2020).

Some new permanent stations installed by Geoscience Australia started operation in WA in 2018. In addition, the Geological Survey of Western Australia installed several semi-permanent stations in the Yilgarn Craton and the Kimberley/Canning Basin region. Several short-period stations, for example, from a 6-month, 6-station rapid deployment following the 2018 Lake Muir earthquake (Clark et al. 2020), and a 8-station, 3-month deployment after the 2022 Arthur River earthquake, also contribute to the current Moho compilation.

Receiver function H-k stacking (Zhu & Kanamori 2000) was utilized to extract the Moho topography in several published models (Yuan 2015, Sippl et al. 2017) that are included in this compilation. For the remaining new stations, Moho depth extracted from depth-migrated receiver functions through a common-conversion-point (CCP) stacking technique has been used to verify the Moho estimates from the H-k method, and to provide a Moho depth estimate when the H-k method does not provide a robust result due to complicated crustal structures (H. Yuan - personal

communication, 2022). For the migration of the time-domain receiver function, the AuSREM crustal P wavespeed V_p (Salmon et al. 2013) is extracted beneath each station, and the V_p/V_s ratio is interpolated from the model covering the whole of Western Australia (Yuan 2015) to extract a shear wavespeed model (V_s).

In reporting the quality of the new Moho depth estimates, we consider that we have robust estimates when: (a), the H-k method shows a unimodal distribution of the Moho depth from 100 bootstrapped datasets, and the Moho depth is clearly observed in a single positive jump in the migrated receiver functions or (b) the H-k analysis shows multiple possible Moho depths, and one of the depths can be matched by the depth-migrated receiver functions. For quality factors (c) and (d), the Moho depth may be estimated by either H-k stacking or depth-migrated receiver functions, but the results are considered less robust. For some stations with short duration of recording or complex crustal structure, as in the Perth Basin, we have been able to extract Moho depth estimates from CCP stacks, but these results are given low weight.

Some additional Moho estimates from refraction studies in the Yilgarn craton to the east of Perth, with both east-west and north-south profiles, are included from Galybin (2006).

3.1.3 AuScope and ANSIR experiments

The AuScope infrastructure project has supported the deployment of portable seismic instrumentation to supplement efforts funded by universities and the Australian Research Council (Figure S1). In conjunction with the AuScope Earth Imaging program, the Australian National Seismic Imaging Resource (ANSIR) has provided seismic equipment to the wider Australian research community, providing further targeted contributions and collaborations. The southern AuScope stations played an important role in extending coverage to the west in the autocorrelogram stack results presented by Kennett et al. (2015) and have also been used by Qashqai et al. (2019) with waveform inversion of autocorrelograms from teleseismic arrivals.

From 2015–2017 a set of 79 stations were deployed in the AQT experiment spanning from northern New South Wales to the Mt. Isa block, linking with earlier portable stations and reflection profiles. These stations mostly lie on relatively thick sediments with somewhat complex receiver function responses. Autocorrelation of teleseismic P and its coda provides estimates of P reflectivity beneath the stations that avoid masking of the transition from crust to mantle (Kennett & Liang 2021). The results tie well with the reflection profiles traversing this area carried out in 2014–2015, and indicate a narrow transition zone between the North Australian Craton and the Thomson Orogen to the south. This boundary probably extends through the full lithosphere.

As can be seen in Figure 2, in central Australia very thick crust appeared to lie in close proximity

to rather thin crust to the east centered upon Lake Eyre, but the nature of the transition had not been investigated in detail. The MAL experiment in 2018–2019 deployed 68 portable stations at approximately 3 km intervals in an east-west line that crosses the edge of the Gawler Craton in South Australia that is masked under sedimentary cover (Liang & Kennett 2020). The dense station spacing allowed common reflection point (CRP) imaging of the P reflection response through the full lithosphere using autocorrelation of teleseismic arrivals. Below the Moho identified from receiver functions there is a transitional zone that pinches out gently at the craton edge.

A further deployment supported by AuScope was undertaken from 2018-2022 within the Lake Eyre Basin in which 40 stations (22 broadband and 18 short-period) were deployed surrounding Kati Thanda–Lake Eyre in north-eastern South Australia (Eakin 2019). This experiment was impacted by Covid related border and travel restrictions causing several interruptions and delays to servicing. Nevertheless, sufficient data has now been retrieved to allow for much improved definition of the Moho across the temporary network, including the region previously identified in Figure 2 with a transition from thicker crust beneath the Gawler Craton to thinner crust towards the east beneath Lake Eyre.

This area of South Australia, particularly towards the north-east of the state, has a complex sedimentary overburden with multiple Phanerozoic sedimentary basins overlain on each other. As a result, receiver function time series are commonly dominated by strong reverberations which can obscure the signals from the crust and mantle (Agrawal et al. 2022). A resonance filter, constructed using the properties of the autocorrelation of the radial receiver function (Yu et al. 2015), proved to be useful in curtailing the sediment reverberation effect and thus aided the detection of the P-to-S conversion from the Moho (Agrawal et al. 2023). Autocorrelation methods have also helped to extract complementary information on crustal thickness in the areas with thick sediment cover.

In tandem with the recent AuScope deployments in South Australia, the Geological Survey of South Australia (GSSA) led the AusArray-SA deployment from 2020-2022 across the eastern-central Gawler Craton (O'Donnell et al. 2020), using instruments supplied from both the AuScope-ANSIR facility and Geoscience Australia. These stations benefited from reduced sediment cover, compared to stations from the Lake Eyre Basin array, allowing for easier identification of the Moho from receiver functions (Agrawal et al. 2023).

AuScope support also allowed the deployment of additional stations in the Kimberley region in northern Western Australia in 2019. Once again, Covid travel restrictions have affected data recovery and data has only recently become available. Results from 8 new stations supplement earlier sparse deployments and provide useful constraints for this remote region (M.S. Miller - personal communication, 2022).

Table 1. Weighting used for multiple datasets

Data type	weight	spatial spread [°]
refraction	0.7	0.80
marine wide-angle	1.0	0.25
receiver functions	1.0	0.50
tomography	1.0	0.60
autocorrelation	1.0	0.55
reflection	1.0	0.25
gravity inversion	0.15	0.40

3.1.4 Surrounding area

To improve the definition of the Moho surface in the north we have included data from the Indonesian Arc from analysis of permanent stations (Fauzi et al. 2021) and a denser network of temporary stations in the Timor area (Zhang & Miller 2021). Australian lithosphere extends into Timor, Roti and Savu, so these islands have a direct connection to the continental model. Some results from stations in Papau New Guinea from Qashqai et al. (2019) are also included.

3.2 Constructing the Moho surface

We have used the Gaussian process scheme developed by Kennett (2019) to allow the fusion of the many different datasets into a single Moho surface. This approach assigns a Gaussian *a priori* spatial influence zone around each point together with a weighting based on the nature of the estimate and its quality. At each sampled point the composite Moho value is a weighted combination of all the different styles of data points that make a non-negligible contribution. As shown in Table 1, different measures of spatial spread are applied for each class of Moho result in an effort to account for the nature of the sampling around the assigned reference point. For example, the S waves used in receiver functions have a tighter sampling beneath a station than for the autocorrelation of P waves. In consequence a slightly smaller spatial spread is used. Within each data class a quality weighting is assigned based on the reliability of the estimate. As a result the influence of a particular data point on the Moho surface comes from the spatial sampling assigned to the data class modulated by the relative quality weight.

We have used all the data points collected for the 2013 compilation, including refraction, receiver functions, reflection profiles and tomography, but have revisited the weightings based on quality. Thus, e.g., historic reflection results have been down-weighted, because it has become clear that the commonly used assumption that the strongest reflection represented the Moho may have been misleading. Indeed in many locations this strong reflector may mark the top of the transition zone

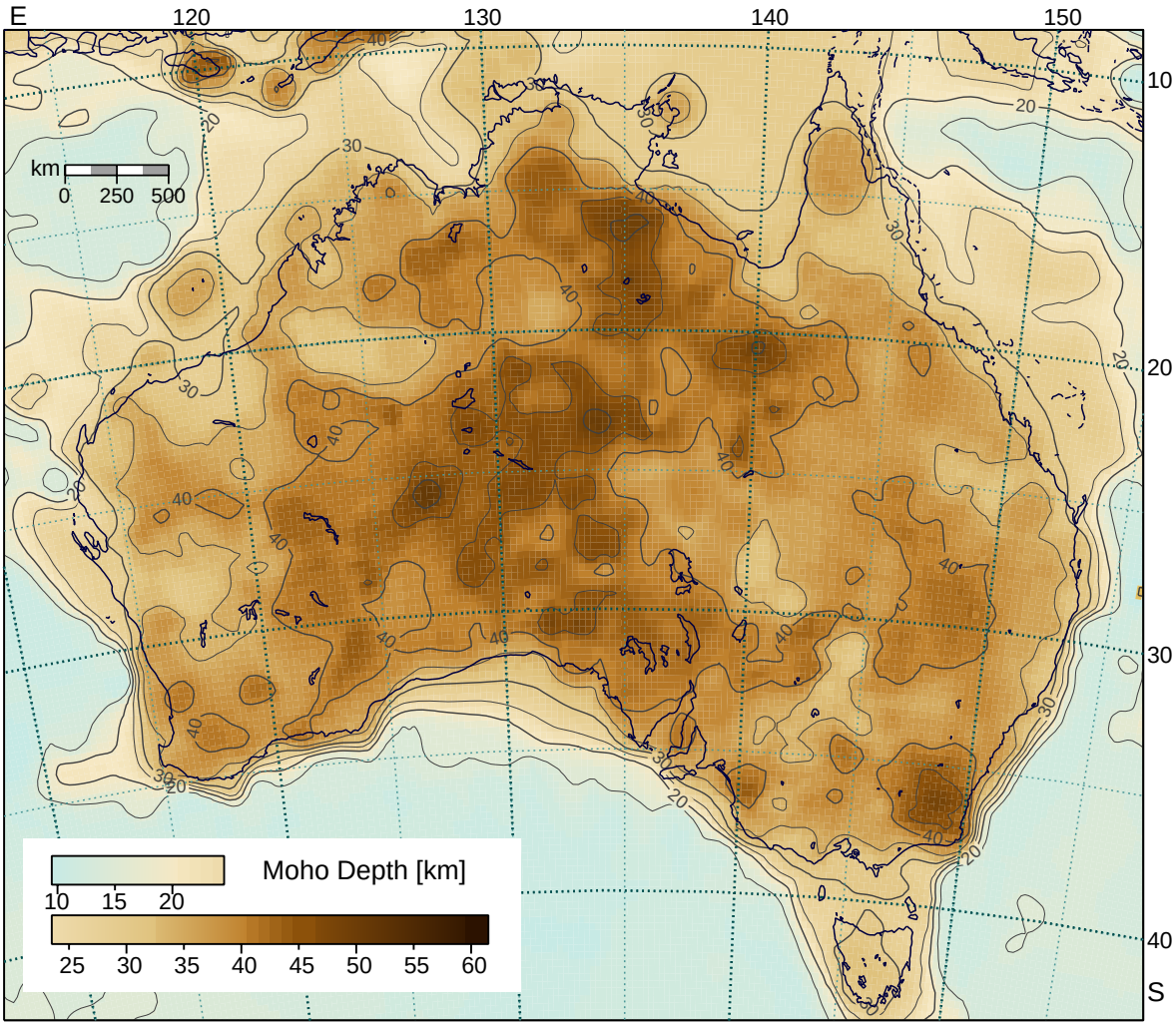

Figure 3. Moho surface constructed using the full suite of data points illustrated in Figure 1, represented using 0.25 degree pixels. The surface has been constructed using the scheme of Kennett (2019) with varying weighting and data influence depending on the type of estimate. Contours at 5 km intervals are also shown.

from crust to mantle. As discussed above, we have also placed lower weight on refraction results and introduced a directional component via two separated data points each of which has a smaller influence zone than that used by Kennett (2019). Within each dataset, each data point is assigned a weighting based on the quality of the Moho result and its consequent likely error. For example, for grading receiver function results using the H-k approach, we use the crustal V_p/V_s ratio in association with the width of the stack peak to assign weights. We have aimed to use consistent relative weightings, but since information comes from many different sources there may be discrepancies. When in doubt we have tended to down-weight observations.

As a background model we have used the Moho model of Aitken et al. (2013) from gravity inversion interpolated onto a 0.5° grid with very low weight (Table 1). With the low weighting this

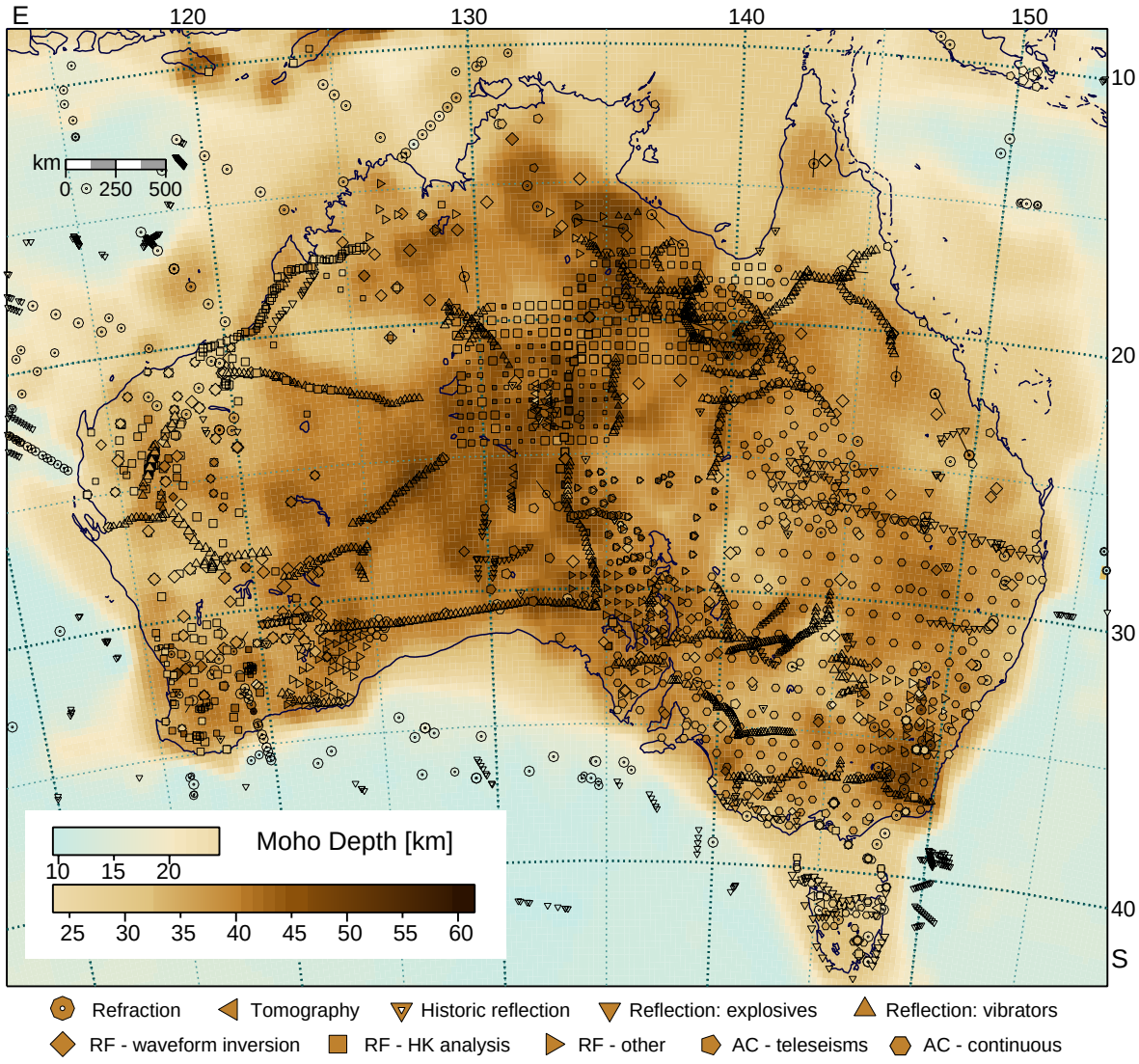

Figure 4. Moho surface constructed using the full suite of data points illustrated in Figure 1, represented using 0.25 degree pixels. The surface has been constructed using the scheme of Kennett (2019) with varying weighting and data influence depending on the type of estimate. The data points from Figure 1 are superimposed with the same colour scheme, so that their relation to the surface can be judged.

background model only makes a significant contribution where other constraints are very weak. The gravity contribution is of particular value in defining the continent-ocean transition since there are very few seismic results in the immediate offshore zone, except on the Northwest Shelf.

The Moho surface constructed from the full set of Moho point values from Figure 1 is displayed in Figure 3 using a 0.25° grid, with contours displayed at 5 km intervals. In Figure 4 we show the Moho surface again, but now with the data points used in the construction superimposed using the same colour scheme as for the grid. Because we have enlarged the range of types of Moho estimates used,

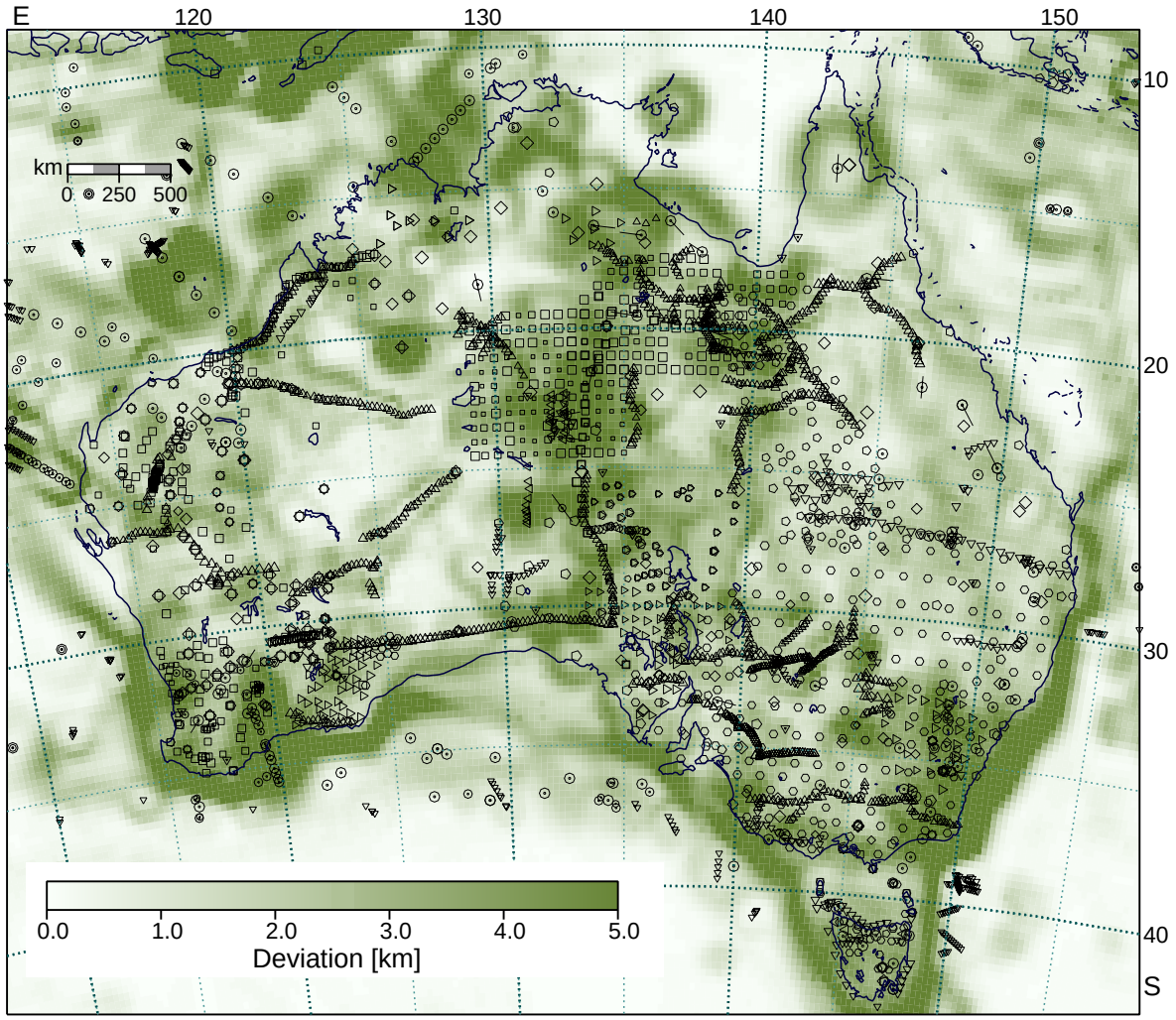

Figure 5. Consistency of Moho estimates using the scheme of Kennett (2019), the square root of the the variance estimate at each 0.25 degree gridpoint is used as the measure of deviation. The data points are superimposed in outline.

the symbol conventions used in Figures 1 and 4 differ from those employed for the earlier estimates in Figure 2.

The addition of many controls on crustal structure in northern central Australia, notably from receiver functions and reflection profiling, has introduced finer-grained structure in the latest model shown in Figures 3 and 4 than seen in the earlier models of Figure 2, though the general trends are maintained. The style of surface construction we have employed means that in the Moho results displayed in Figures 3 and 4 there is much less extrapolation from isolated points than in the 2003 or 2013 models. In Eastern Australia, the addition of autocorrelation results has significantly improved the density of data coverage in the south, though eastern Queensland has as yet only a sparse coverage away from reflection profiles.

The Moho surface of Aitken et al. (2013) used as a low level background was prepared using the available seismic constraints at the time, and has a similar character to the model displayed in Figure 2b. Where the background dominates there is a tendency for apparently thinner crust. In the Canning Basin in Western Australia, this may well be justified since it is also suggested by ambient noise analysis (Y. Chen - personal communication, 2022). However, for areas in the north of Australia such as Arnhem Land and the Cape York Peninsula the limited seismic constraints suggest that Moho thickness may be underestimated.

The surface construction scheme of Kennett (2019) allows an estimate of the local consistency of the Moho values. With the same spatial and data weighting a local variance value can be extracted and its square-root employed as a consistency measure. Figure 5 displays the variation of the consistency of the Moho estimates across the continent using this approach. The continent-ocean transition in the southern part of Australia shows significant inconsistency because the Moho on the continent and ocean sides occur at very different depths. Other complications occur in central Australia where strong changes in crustal thickness associated with major gravity anomalies lie in narrow east-west bands. Such variations are hard to capture with a symmetric influence domain around each data point. Zones of rapid change in Moho depth at the northern edge of the South Australian craton also display significant variability. In southeastern Australia some Moho estimates appear to pick up the top of the gradient zone between crust and mantle leading to a slight underestimate of crustal thickness and locally strong variability.

Isolated data points tend to have a 'halo' of inconsistency that marks the transition from the spatial influence zone of the point to the background model. In a few locations different styles of analysis have produced notably different estimates of crustal thickness and these appear as solid spots. In general there is good consistency between the results obtained with many different analysis methods and classes of observational data, particularly across the continental area.

In the Supplementary Material (Section S3) we show comparisons of the current results with other studies: the work of Qashqai et al. (2019) using waveform inversion of teleseismic correlations at over 1200 stations and Birkey et al. (2021) who have employed teleseismic receiver function stacking directed primarily at the exploitation of Sp results, but also including Ps, for a total of 35 permanent stations.

For each comparator data set there is good general agreement with the Moho surface constructed from the full dataset assembled here, with Moho estimates for most stations lying within ± 3 km for incident P waves. In each case there are a few discordant stations, but none are in common.

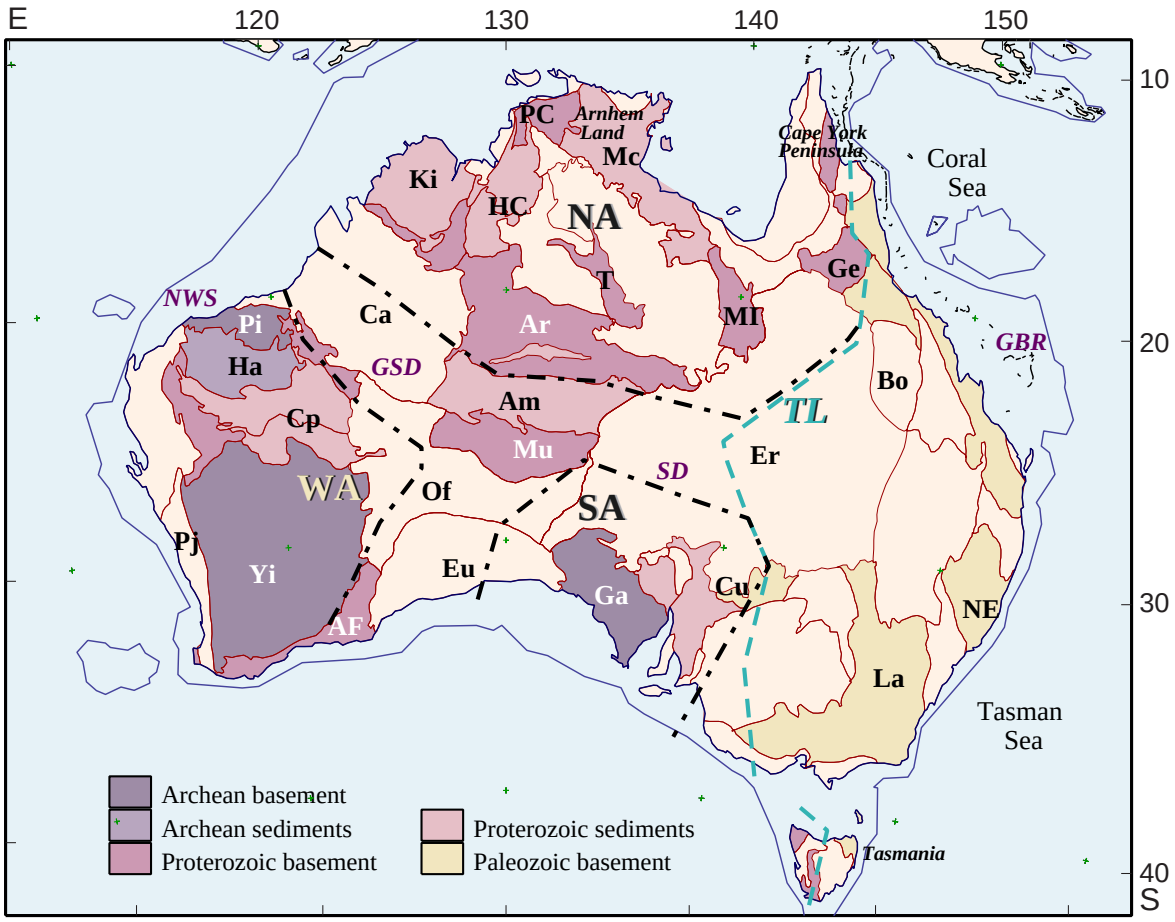

Figure 6. Simplified relationships of major tectonic features of Australia. The outlines of the major cratons are indicated: WA – West Australian Craton, NA – North Australian Craton, SA – South Australian Craton, and TL – the Tasman Line marking the limit of Precambrian exposure. Marked features: AF – Albany–Fraser Orogen, Ar – Arunta Block, Am – Amadeus Basin, Bo – Bowen Basin, Ca – Canning Basin, Cp – Capricorn Orogen, Cu – Curnamona Craton, Er – Eromanga Basin, Eu – Eucla Basin, Ga – Gawler Craton, Ge – Georgetown Inlier, Ha – Hamersley Basin, HC - Halls Creek Belt, Ki – Kimberley block, La – Lachlan Orogen, Mc – MacArthur Basin, MI – Mt Isa Inlier, Mu – Musgrave Orogen, NE – New England Orogen, Of – Officer Basin,PC – Pine Creek Inlier, Pi – Pilbara Craton, Pj – Pinjarra Orogen, T – Tennant Creek Inlier, Yi – Yilgarn Craton; *SD* – Simpson Desert, *GSD* – Great Sandy Desert, *GBR* – Great Barrier Reef, *NWS* – North West Shelf.

4 DISCUSSION

In the last ten years additional seismological data has significantly improved the rendering of the Moho across the Australian continent. Full-crustal reflection profiles and further passive seismic deployments in areas with substantial sediment cover have made a major difference. Yet there are still areas with limited coverage. The Canning Basin has good control near the coast, but the interior is barely sampled

since data collection in the western deserts has focused on a limited number of transport corridors. The northernmost regions of Australia are also under sampled.

The 2003 compilation (Figure 2a), using just refraction results and receiver functions from the reconnaissance SKIPPY project, delineated many of the major features. Subsequent studies have provided substantial infill and also notable modifications in some areas. An example is the Albany-Fraser Orogen in Western Australia (see Figure 6). Early indications of a thin crust were found to correlate with the top of a zone of rather high wavespeed material at the base of the crust with a further discontinuity below (Gorbatov et al. 2013). Full-crustal reflection profiling and dense passive seismic work (Sippl et al. 2017) reveal localised thickening of the crust in a transition zone at the edge of the Yilgarn Craton.

Such crustal thickening at the edges of the cratons can be recognised in a number of locations. The very long reflection profile that crosses the Nullabor Plain from the Yilgarn Craton to the Gawler Craton in South Australia revealed unexpected deepening of the Moho on the edge of the Gawler Craton, under cover (Dutch et al. 2015). At the northern edge of the Yilgarn Craton, there is an indication of crustal thickening by underthrusting and similar imbricate structures are preserved on the western margin as well (Kennett & Saygin 2015). The crustal thickening is quite localised and so is likely to be missed unless sampling across the margin is quite dense. Studies in eastern Canada across the boundary between the Superior Craton and the Grenville Orogen show some similarities with localised zones of thickening adjacent to the transition (Cook et al. 2010, Darbyshire et al. 2017).

Within portions of a craton with a common initial age and tectonic history, the character of the Moho tends to be relatively coherent with modest changes in depth and clarity. But, there can be significant change within zones with similar material at the surface including localised steps in the reflection Moho of several kilometres (see, e.g., Kennett & Saygin 2015). Although we have allowed a tight zone of spatial influence for results from reflection work, it is inevitable that such jumps will be somewhat suppressed especially when there is influence from passive receiver-based approaches with much less spatial resolution.

For stations in central Australia, the character of teleseismic receiver functions differs notably for events to the north and east. This difference reflects the east-west grain of the major structures, associated with substantial gravity anomalies. In this area the base of the crust also shows a gradient zone into the mantle rather than any distinct interface. It is, therefore, hard to capture the entire character of the variation of the transition between crust and mantle with a single Moho surface. The present model attempts to take account of the nature of each of the Moho estimates, rather than make local averages as used in Kennett et al. (2011) and Salmon et al. (2013). In this way we have

aimed to preserve as much of the local character as possible, whilst providing a suitable rendering of the broad-scale behaviour in areas with limited data coverage.

One of the areas where the current Moho distribution differs significantly from the results shown in Figure 2 is in southern central Australia, around the Lake Eyre Basin, where previously the patterns were controlled by just a few scattered data points of limited quality. With the additional data collected in recent years, a significant contrast in crustal thickness remains but the differences in crustal thickness between the cratonic zone ($\sim$ 45–50 km) and the basin region to its east ($\sim$ 30–35 km) have been reduced. With the new Moho estimates the position of the relatively sharp transition to thinner crust has shifted further east in better accord with the edge of the Gawler Craton inferred from magnetic and other studies (see, e.g., Liang & Kennett, 2020). This Moho transition lies well to the west of most estimates of the location of the Tasman Line (Direen & Crawford 2003, Kennett et al. 2004), based on a variety of different premises, and does not align with any inferred crustal lineaments.

Chen & Saygin (2020) have developed an approach that allows the use of both synchronous and asynchronous station networks to be used for ambient noise tomography. This procedure has been applied to the many different temporary networks across Australia (Section S1 in the Supplementary Materials), in conjunction with the backbone of permanent stations to produce a high-definition shear wavespeed model extending well into the upper mantle (Y. Chen - personal communication, 2022). The estimates of Moho depth extracted from this tomographic model for the Lake Eyre region fit well with our new compilation; with thicker crust than in earlier Moho models and a similar transition to slightly thinner crust.

The various data sets that we have employed in the construction of the Moho surface respond to different aspects of the crust–mantle transition. Receiver function methods exploit conversions between P and S waves from teleseismic arrivals, which are most pronounced for discrete velocity jumps. The conversions between P and S from a gradient in seismic wavespeeds are weak, with the largest effects associated with the top and bottom of the gradient zone. As a result, there can be a tendency for receiver-function Moho depths to be shallower than those obtained by other methods, because the top of a gradient zone has been registered. In reflection profiling and autocorrelation studies we concentrate on changes in the reflectivity patterns, without a direct link to upper-mantle velocities.

The character of the Moho from reflection and receiver function studies is summarised in Figure 7. We display both the quality of picks from reflection studies (Kennett et al. 2016, Doublier et al. 2022) and the estimated thickness of transition from crust to mantle from receiver function studies. The measure for the quality of reflection pick is somewhat subjective, but since all records have been

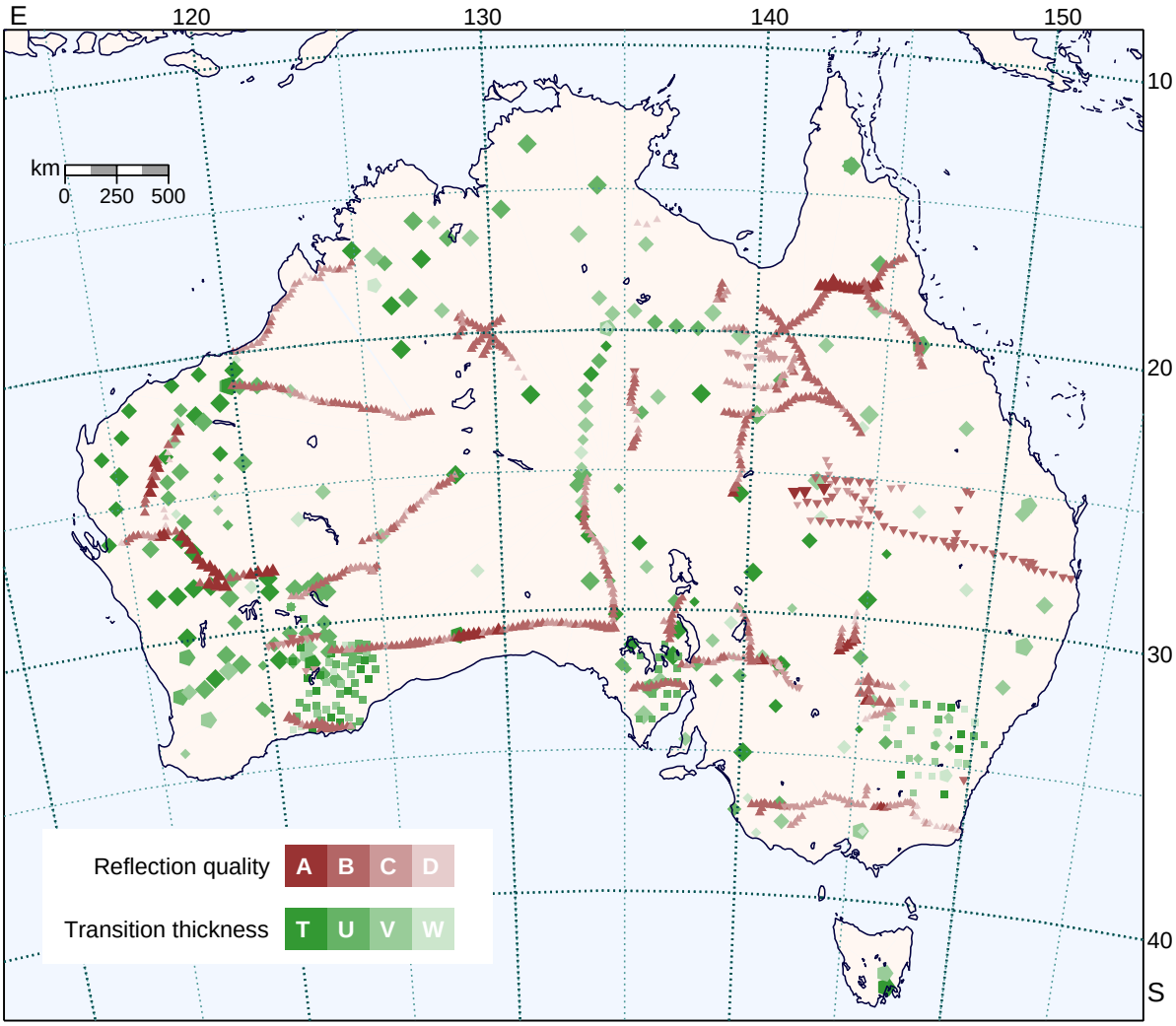

Figure 7. The nature of the crust-mantle transition from different classes of information: (i) Reflection clarity based on the quality of picking the Moho from published record sections: A – clear and sharp to D – weak and indistinct. (ii) The thickness of the crust–mantle transition estimated from receiver function studies, T: < 2 km, U: 2–4 km, V: 4–8 km, W: > 8 km. As in Figures 4 and 5 the size of symbols increases with the reliability of the results.

picked by the same people in a similar way the relative variations will be caught. We use a coding from A–D, following Kennett & Saygin (2015): Class A – very sharp reflections marking the base of reflectivity; Class B – a distinct change in character with depth, but the actual base of reflectivity is more difficult to pick; Class C – the reflectivity fades downwards so that the Moho is rather nebulous and difficult to pick, even though the general location is evident; Class D – no clear reflections in the vicinity of the Moho (Class D), even though it has been visible elsewhere on the profile. Examples of record sections of segments of full-crustal reflection profiles with a range of Moho character are presented in Kennett & Saygin (2015).

We also use four categories for the estimated thickness of the transition between crust and mantle from receiver functions (T: $<$ 2 km, U: 2–4 km, V: 4–8 km, W: $>$ 8 km). The transition thickness estimates displayed in Figure 7 have mostly been extracted from waveform inversions in which the P wavespeed at the top and bottom of the transition and the thickness are direct parameters. These values are shown with diamond symbols, the smaller square symbols are based on estimates provided by the authors of the studies.

Where both estimates can be made, the two different measures of Moho character are in general agreement, because a sharp Moho transition will be associated with a very clear reflection, whereas a gradational structure has less marked reflectivity. In each case the size of symbols increases with the reliability of the results.

The largest concentration of sharp crust-mantle transitions is in the western cratons, but even here there is noticeable local variability. There is no obvious relation between the character of the Moho and crustal age. Though intact Archean crust, which has not been affected by later basin development, magmatism and thrusting, tends to have a relatively well defined Moho. A gradient zone at the base of the crust is not uncommon in Proterozoic northern Australia and in southeastern Australia. In each case this is likely to be associated with intrusion of mafic material into the lowermost crust. In such scenarios the reflection signature for the Moho can almost vanish (Kennett & Saygin 2015).

The general behaviour of Moho depth across the continent is illustrated in Figure 8, using a simplified division into six categories. The division aims to capture the differing nature of the crust. We have separated out the principal cratonic zones and their surroundings. We here use all receiver function, autocorrelation and reflection results together, since within the restrictions imposed by different coverage the datasets are concordant (see Supplementary Material, Figure S7). The violin plots display the full distribution of the Moho depth estimates for each province, as a probability distribution, accompanied by indicators of the median and the inter-quartile range.

In Western Australia we have separated the Pilbara Craton from the Yilgarn because of their contrasting behaviour of crustal thickness. Most results from the ancient Archean Pilbara show Moho depth shallower than 35 km (median 32.5 km) with a sharp transition at the base of the crust (Figure 7). The inter-quartile band for the Yilgarn does not overlap with that for the Pilbara and the median depth is 39.3 km. Both the North Australian and South Australian Cratons, dominated by Proterozoic material, have mostly slightly thicker crust than the Yilgarn. At the margins of the cratonic areas the crust tends to thicken, complicating any choice of division.

The Proterozoic mobile belts surrounding the main cratonic elements tend to have thicker crust, but the situation is complicated by the strong east-west bands of uplifted crust in Central Australia that are responsible for the dominant gravity anomalies. The thickest crust, and so deepest Moho, is

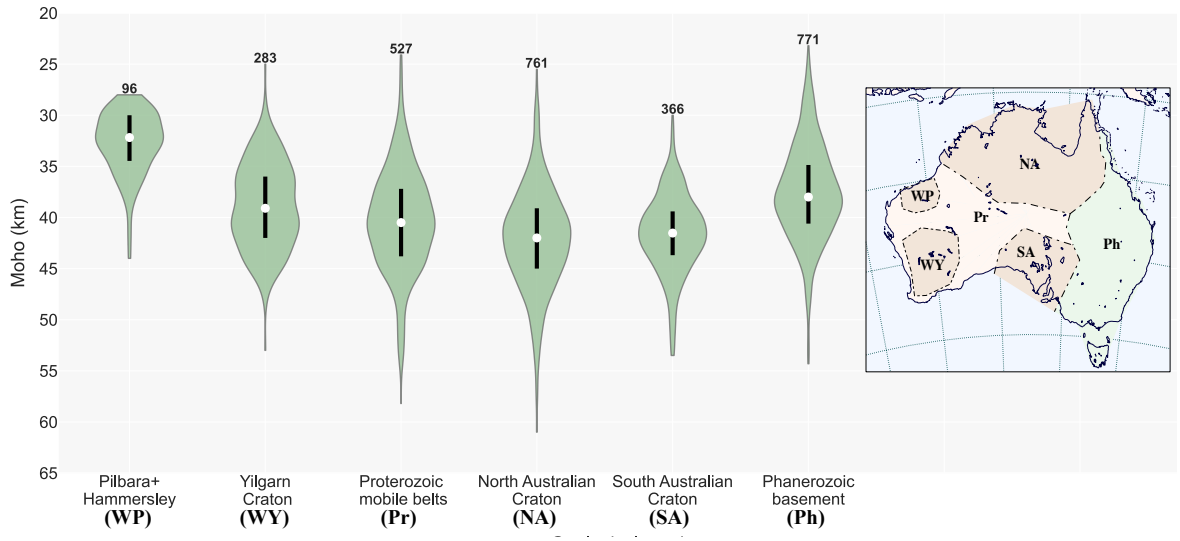

Figure 8. Moho depth distribution for continental Australia expressed as violin plots. Australia is divided into six provinces based on age and geological history (as in insert map). Each violin plot displays the full distribution of the Moho estimates in depth with the median shown as a white circle and the interval between the second and third quartiles with a black bar.

limited to zones where there is a gradational transition from crust to mantle, most likely linked to mafic intrusion into the lowermost crust. Such basal gradient zones occur in the North Australian Craton and Proterozoic mobile belts, as well as in parts of the Lachlan Fold Belt in the southeast with Phanerozoic crust.

Even with improved sampling across the continent, the distribution in the violin plots are rather broad with a significant span between the second and third quartiles. There are regions within each domain that show rather coherent behaviour with similar Moho character, but in aggregate the zones span significant variations in surface character so it is not surprising to see variation at depth. It may be possible to obtain tighter constraints by subdividing the continent more finely, but the choice of domains in 3-D is not simple (e.g., Korsch & Doublier 2015).

The pattern of Moho depths illustrated in Figure 8, suggests more change between the early Archean of the Pilbara (WP) and the later Yilgarn (WY) than to the dominantly Proterozoic zones (Pr, NA, SA). On the whole the Phanerozoic areas show thinner crust than the Proterozoic, but with localised thickening. The overall behaviour is not unlike that summarised by Tugume et al. (2013) for Africa and Arabia, but their Moho depths derived from gravity inversion are slightly shallower than their Australian counterparts. As noted by Derbyshire et al. (2017) the Archean domains of eastern and northern Canada show broadly similar Moho depth and seismic structure across regions spanning $>$ 1000 km. The somewhat greater variation seen in Australia appears to be linked to denser sampling, but

is still consistent with relatively uniform crustal formation processes across the later Archean. Modest contrasts in crustal properties for the Proterozoic could reflect a change in crustal processes. However, arguments for secular change depend on the debatable assumption that the age of the last crustal growth event at the base of the crust is correlated to the surface age, and also require an understanding of possibly modifications related to later tectonic events (such as orogenies and rifting).

In some regions there are clear indications of variation in crustal structure and Moho depth that link to changes in crustal age. Within the Yilgarn Craton of Western Australia, Reading et al. (2007) have noted a progression in crustal structure with greater Moho depth associated with older parts of the craton in the west. This behaviour is quite similar to that proposed by Thompson et al. (2010) for the region around Hudson Bay in Canada.

5 CONCLUSIONS

The extensive deployments of portable seismometers across Australia in the last decade, together with several thousand extra kilometres of seismic reflection profiling have markedly improved the sampling of the Moho. Autocorrelation techniques have supplemented conventional receiver functions extracted from teleseismic recordings and have proved valuable in areas of sedimentary cover with strong contrasts. The result is a more detailed delineation of the variations in the depth to Moho and the character of the crust-mantle transition. In many areas we have multiple constraints derived from different techniques that show good consistency, so that we can have confidence in the general patterns of Moho depth. There remain a number of areas particularly in the north of the continent where sampling is rather sparse, and it is to be hoped that future experiments will improve coverage. In Western Australia a major initiative has begun with the aim of deploying portable seismic sites at 40 km spacing across the entire state over the next decade. There will be formidable logistic hurdles to overcome, particularly in the desert areas, but in time the region will have the densest consistent coverage in the whole continent.

As noted by Kennett et al. (2011) the distribution of Moho depth does not show any simple dependence on the age of the basement or the surface rocks (Figure 8). Improved coverage in central Australia means that the seismic results now pick up the major east-west features with Moho steps that are very prominent in the gravity field (see, e.g., Kennett et al. 2018 - Chapter 5). With the use of a surface construction scheme that can take account of the differing spatial sampling and resolution of the various types of dataset, we are able to preserve localised features more effectively than with the broad scale interpolation used in the earlier studies. This means that the continent-wide Moho surface provides a good basis for regional studies. Where a finer local grid is desired the suite of Moho points can be used with the Kennett (2019) scheme to extract the requisite estimates.

RESOURCES

The Moho model at 0.25 degree resolution and the complete set of Moho estimates, organised by the technique employed, are to be found at the AusPass repository (http://auspass.edu.au/research/Moho). The full set of references for the sources of information used in the Moho compilation are provided in the Supplementary Material.

ACKNOWLEDGMENT

The AusMoho project represents a continuation of the development of the Australian Seismological Reference Model (AuSREM) supported by AuScope (auscope.org.au) via the National Collaborative Research Infrastructure Strategy (NCRIS) of the Australian Government. The AusPass repository is also enabled by AuScope through the NCRIS program.

The compilation used here relies on data collected by many different institutions and agencies. The refraction studies were mostly made by the Bureau of Mineral Resources (now Geoscience Australia). The first phase of portable station deployments was made by the Australian National University with subsequent support from Australian Research Council grants and AuScope through the NCRIS program. Major contributions have been made by Geoscience Australia in the Exploring for the Future project, the Geological Survey of Western Australia, the Institute of Geology and Geophysics of the Chinese Academy of Science in joint experiments in Western Australia, and the Geological Survey of South Australia. Reflection profiles were mostly coordinated by Geoscience Australia, with additional support from State and Territory Geological Surveys and AuScope.

SA and CE are supported by Australian Research Council Grant DE190100062. This paper is published with permission from the Chief Executive Officer, Geoscience Australia, and the Executive Director, Geological Survey of Western Australia.

REFERENCES

Agrawal, S., Eakin, C.M. & O'Donnell, J.P., 2022. Characterizing the depth of cover across South Australia: A simple passive-seismic method for estimating sedimentary thickness, *Geophys. J. Int.*, **231**, 1850–1864. doi: 10.1093/gji/ggac294

Agrawal, S., Eakin, C.M. & O'Donnell, J.P., 2023. Tracking crustal thickness at the sediment inundated edge of the Gawler Craton, South Australia, *Tectonophysics*, in review. Available at SSRN: doi: 10.2139/ssrn.4285912

AMIRA (Australian Mineral Industries Research Association), 2017. *Unlocking Australia's hidden potential*, AMIRA, Melbourne.

Aitken, A.R.A., Salmon, M.L. & Kennett, B.L.N. 2013. Australia's Moho: A test of the usefulness

of gravity modelling for the determination of Moho depth, *Tectonophysics*, **609**, 468–479. doi: 10.1016/j.tecto.2012.06.049

Balfour, N.J., Salmon M. & Sambridge, M., 2014. The Australian Seismometers in Schools network: education, outreach, research, and monitoring, *Seism. Res. Lett.*, **85**, 1063–1068. doi: 10.1785/0220140025

Bodin, T., Kennett, B.L.N., Salmon, M. & Sambridge, M. 2012. Probabilistic surface reconstruction from multiple data-sets – an example for the Australian Moho, *J. Geophys. Res. B*, **117**, B10307. doi: 10.1029/2012JB009547

Bello M., Cornwell D.G., Rawlinson N., Reading A.M. & Likkason O.K., 2021. Crustal structure of southeast Australia from teleseismic receiver functions, *Solid Earth*, **12**, 463–481. doi: 10.5194/se-12-463-2021

Birkey, A., Ford, H.A., Dabney, P. & Goldhagen, G., 2021. The lithospheric architecture of Australia from seismic receiver functions. *J. Geophys. Res.: Solid Earth*, **126**, e2020JB020999. doi: 10.1029/2020JB020999

Betts, P.G., Giles, D., Lister, G.S. & Frick, L.R., 2002. Evolution of the Australian Lithosphere, *Austral. J. Earth Sci.*, **49**, 661–692. doi: 10.1046/j.1440-0952.2002.00948.x

Chen, Y., Niu, F., Liu, R., Huang, Z., Tkalčić, H., Sun, L. & Chan, W., 2010. Crustal structure beneath China from receiver function analysis. *J. Geophys. Res.*, **115**, 1–22. doi: 10.1029/2009JB006386

Chen, Y. & Saygin, E.,2020. Empirical Green's function retrieval using ambient noise source-receiver interferometry. *J. Geophys. Res.: Solid Earth*, **125**, e2019JB018261. doi: 10.1029/2019JB018261

Clark, D.J., Brennand, S., Brenn, G., Allen, T.I., Garthwaite, M.C. & Standen, S., 2020. The 2018 Lake Muir earthquake sequence, southwest Western Australia: rethinking Australian stable continental region earthquakes, *Solid Earth*, **11**, 691-717. doi: 10.5194/se-11-691-2020

Clitheroe, G., Gudmundsson, O. & Kennett, B.L.N., 2000. The crustal thickness of Australia, *J. Geophys. Res.*, **105**, 13 697–13 713. doi: 10.1029/1999JB900317

COAG (Council of Australian Governments), 2017. *National Mineral Exploration Strategy*, http://www.coagenergycouncil.gov.au/publications/nationalmineral-exploration-strategy-december-2012.

Collins, C.D.N., 1991. The nature of the crust-mantle boundary under Australia from seismic evidence, *The Australian Lithosphere*, edited by B.J. Drummond, Spec. Publ., Geol. Soc. Aust., **17**, 67–80.

Collins C.D.N., Drummond B.J. & Nicoll M.G., 2003. Moho depth patterns in the Australian continent, 121–128, in *The Evolution and Dynamics of the Australian Plate*, Ed. D. Müller & R. Hillis. Geological Society of Australia Special Publication **22** and Geological Society of America Special Paper **372**. doi: 10.1130/0-8137-2372-8.121

Cook, F.A., White, D.J., Jones, A.G., Eaton, D.W.S., Hall, J. & Clowes, R.M., 2010. How the crust meets the mantle: Lithoprobe perspectives on the Mohorovičić discontinuity and crust–mantle transition. *Canadian J. Earth Sciences*, **47**, 315–351. doi: 10.1139/E09-076

Czarnota K., Hoggard M. J., White N. & Winterbourne J., 2013. Spatial and temporal patterns of Cenozoic dynamic topography around Australia, *Geochem. Geophys. Geosyst.*, *14*, 634—658, doi:10.1029/2012GC004392

Darbyshire, F.A., Bastow, I.D., Petrescu, L., Gilligan, A. & Thompson, D.A. 2017. A tale of two orogens: crustal processes in the Proterozoic Trans-Hudson and Grenville Orogens, eastern Canada, *Tectonics*, **36**, 1633—1659, doi:10.1002/2017TC004479

Dentith, M., Yuan, H., Murdie, R.E., Pina-Varas, P., Johnson, S.P., Gessner, K. & Korhonen, F.J., 2018. Improved interpretation of deep seismic reflection data in areas of complex geology through integration with passive seismic data sets. *J. Geophys. Res.: Solid Earth*, **123**, 10 810-10 830 doi: 10.1029/2018JB015795

Direen, N.G. & Crawford, A J., 2003. The Tasman Line: where is it, what is it, and is it Australia's Rodinian breakup boundary?, *Austral. J. Earth Sci.*, **50**, 491–502. doi: 10.1046/j.1440-0952.2003.01005.x

Dooley, J.C. & Moss, F.J. 1988. Deep crustal reflections in Australia 1957-1973 – II. Crustal models, *Geophys. J. R. Astr. Soc.*, **293**, 239–249. doi: 10.1111/j.1365-246X.1988.tb01999.x

Doublier, M.P., Gessner, K., Johnson, S.P., Kelsey, D.E., Haines, P.W., Howard, H.M., Chopping, R., Smithies, R.H., Hickman, A.H., Martin, D.McB., Southby, C., Champion, D.C., Huston, D.L., Calvert, A.J., Gorczyk, W., Kohanpour, F., Moro, P., Costelloe, R., Fomin, T., Yuan, H. & Kennett, B.L.N. 2022, Interpretation of the basement component of seismic line 18GA-KB1, in Carr, L.K., Southby, C., Edwards, D.S., Anderson, J.R. & MacFarlane, S.K. (eds) *Exploring for the Future: Canning Basin: Kidson Seismic survey (18GA-KB1) and geological interpretation*. Geoscience Australia Record 2022/16, 35–48

Dutch, R.A., Pawley, M.J. & Wise, T.W. (editors), 2015. *What lies beneath the Western Gawler Craton? 13GA-EG1 Seismic and Magnetotelluric Workshop 2015 — extended abstracts*: Department of State Development, South Australia, Report Book 2015/00029, 84p

Eakin, C.M., 2019. Seismicity, Minerals, and Craton margins: The Lake Eyre Basin Seismic Deployment. *ASEG Extended Abstracts*, **1**, 1–2. doi:10.1080/22020586.2019.12072989

Fauzi, M.F., Anggraini, A., Riyanto, A., Ngadmanto, D. & Suryanto, W., 2021. Crustal thickness estimation in Indonesia using receiver function method, *IOP Conf. Series: Earth and Environmental Science*, **873**, 012086 doi:10.1088/1755-1315/873/1/012086

Ford, H.A., Fischer, K.M., Abt, D.L., Rychert, C.A. & Elkins-Tanton, L.T., 2010. The lithosphere-asthenosphere boundary and cratonic lithospheric layering beneath Australia from *Sp* wave imaging, *Earth Planet. Sci. Lett.*, **300**, 299–310. doi: 10.1016/j.epsl.2010.10.007

Galybin, K.A., 2006. *P-wave Velocity Model for the Southwest of the Yilgarn Craton, Western Australia and its Relation to the Local Geology and Seismicity*, Ph.D. thesis, University of Western Australia.

Geoscience Australia, 2021. Australian National Seismograph Network Data Collection. *Geoscience Australia, Canberra.* doi: 10.26186/144675

Gorbatov, A., Kennett, B.L.N. & Saygin, E., 2013. Crustal properties from seismic station autocorrelograms, *Geophys. J. Int.*, **192**, 861–870. doi: 10.1093/gji/ggs064

Gorbatov, A., Czarnota, K., Hejrani, B., Haynes, M., Hassan R., Medlin, A., Zhao, J., Zhang, F., Salmon, M., Tkalčić, H., Yuan, H., Dentith, M., Rawlinson, N., Reading, A.M., Kennett, B.L.N., Bugden, C. & Costelloe, M., 2020a. AusArray: towards updatable, national high-resolution seismic velocity models of the lithosphere.

In: Czarnota, K., Roach, I., Abbott, S., Haynes, M., Kositcin, N., Ray, A. & Slatter, E. (eds.), *Exploring for the Future: Extended Abstracts*, Geoscience Australia, Canberra. doi: 10.11636/135284

Gorbatov, A., Medlin, A., Kennett, B.L.N., Doublier, M.P., Czarnota, K., Fomin, T. & Henson, P., 2020b. Moho variations in northern Australia. In: Czarnota, K., Roach, I., Abbott, S., Haynes, M., Kositcin, N., Ray, A. & Slatter, E. (eds.), *Exploring for the Future: Extended Abstracts*, Geoscience Australia, Canberra. doi: 10.11636/135179

Grad, M., Tiira, T. & ESC Working Group, 2009. The Moho depth map of the European Plate, *Geophys. J. Int.*, **176**, 279–292. doi: 10.1111/j.1365-246X.2008.03919.x

Kennett, B.L.N., Fishwick, S., Reading, A.M. & Rawlinson, N., 2004. Contrasts in mantle structure beneath Australia – relation to Tasman Lines?, *Austral. J. Earth Sci.*, **51**, 563–569. doi: 10.1111/j.1400-0952.2004.01075.x

Kennett B.L.N., Salmon M., Saygin E. & AusMoho Working Group, 2011. AusMoho: the variation in Moho depth in Australia, *Geophys. J. Int.*, **187**, 946–958. doi: 10.1111/j.1365-246x.2011.05194.x

Kennett, B.L.N. & Saygin, E., 2015. The nature of the Moho in Australia from reflection profiling: A review, *GeoResJ*, **5**, 74–91. doi: 10.1016/j.grj.2015.02.001

Kennett, B.L.N., Saygin, E. & Salmon, M., 2015. Stacking autocorrelograms to map Moho depth with high spatial resolution in southeastern Australia, *Geophys. Res. Lett.*, **42**, 3839–3846. doi: 10.1002/2015GL065345

Kennett, B.L.N., Saygin, E., Fomin, T. & Blewett, R.S., 2016, *Deep Crustal Seismic Reflection Profiling Australia 1978–2015*, ANU Press, Canberra. doi: 10.22459/dcsrp.11.2016

Kennett, B.L.N., Chopping R. & Blewett, R., 2018. *The Australian Continent: A Geophysical Synthesis*, ANU Press. doi: 10.22459/AC.08.2018

Kennett, B.L.N., 2019. Areal parameter estimates from multiple datasets, *Proc. R. Soc. A*, **475**, 20190352. doi: 10.1098/rspa.2019.0352

Kennett, B.L.N. & Liang, S., 2021. The transition from the Thomson Orogen to the North Australian Craton from seismic data. Australian Journal of Earth Sciences, 68, 628-640. doi: 10.1080/08120099.2021.1837955

Korsch, R.J. & Doublier, M.P., 2015. Major crustal boundaries of Australia, and their significance in mineral systems targeting, *Ore Geol. Rev.*, **76**, 211–228. doi: 10.1016/j.oregeorev.2015.05.010

Lambeck, K., Burgess, G. & Shaw, R.D., 1988. Teleseismic travel-time anomalies and deep crustal structure in central Australia, *Geophys. J. R. Astr. Soc.*, **94**, 105–124. doi: 10.1111/j.1365-246X.1988.tb03431.x

Liang, S. & Kennett, B.L.N., 2020. Passive seismic imaging of a craton edge – Central Australia, *Tectonophysics*, **797**, 228662. doi: 10.1016/j.tecto.2020.228662

McQueen, H.W.S. & Lambeck, K., 1996. Determination of crustal structure in central Australia by inversion of traveltime residuals, *Geophys. J. Int.*, **126**, 645–662. doi: 10.1111/j.1365-246X.1996.tb04696.x

Miller, M.S., Pickle, R., Murdie, R., Yuan, H., Allen, T.I., Gessner, K., Kennett, B.L.N. & Whitney, J., 2023. Southwest Australia Seismic Network (SWAN): recording earthquakes in Australia's most active seismic zone, *Seism. Res. Lett.*, **94**, doi: 10.1785/0220220323.

Mohorovičić, A., 1910. Das beben von 8 Okt. 1909, *Jahrb. Meteorol. Obs. Agram (Zagreb)*, **9**, Teil IV.

Moss, F.J. & Dooley, J.C., 1988. Deep crustal reflection recordings in Australia 1957-1973 – I. Data acquisition and presentation, *Geophys. J. R. Astr. Soc.*, **293**, 229–238. doi: 10.1111/j.1365-246X.1988.tb01998.x

Murdie, R., Yuan, H., Dentith, M.C. & Lin, X., 2020a. A passive seismic experiment in the Perth Basin, Western Australia. *Geological Survey of Western Australia, Report 208*. doi: 10.1080/14432471.2020.1828423

Murdie, R., Gessner, K., Miller, M., Salmon, M., Yuan, H., Whitney, J., Gray, S. & Allen T., 2020b. Geological Survey of Western Australia: SWAN takes off - a new seismic monitoring project in Western Australia, *Preview* **208**, 28–29. doi: 10.1080/14432471.2020.1828423

O'Donnell, J.P., Thiel, S., Robertson, K., Gorbatov, A. & Eakin, C. 2020. Using seismic tomography to inform mineral exploration in South Australia: the AusArray SA broadband seismic array, *MESA Journal*, **93**, 24–31. doi: 10.1080/14432471.2021.1935718

Qashqai, T.M., Saygin E. & Kennett B.L.N. 2019. Crustal imaging with Bayesian inversion of teleseismic P-wave coda autocorrelation, *J. Geophys. Res.: Solid Earth*, **124**, 5888–5906. doi: 10.1029/2018JB017055

Rawlinson, N., Tkalčić, H. & Reading, A.M., 2010. Structure of the Tasmanian lithosphere from 3D seismic tomography, *Austral. J. Earth Sci.*, **57**, 381–394. doi: 10.1080/08120099.2010.481325

Reading, A.M., Kennett, B.L.N. & Dentith, M.C. 2003. The seismic structure of the Yilgarn Craton, Western Australia, *Austral. J. Earth Sci.*, **50**, 427–438. doi: 10.1046/j.1440-0952.2003.01000.x

Reading, A.M. & Kennett, B.L.N., 2003. Lithospheric structure of the Pilbara Craton, Capricorn Orogen and northern Yilgarn Craton, Western Australia, from teleseismic receiver functions, *Austral. J. Earth Sci.*, **50**, 439–445. doi: 10.1046/j.1440-0952.2003.01003.x

Reading, A.M., Kennett, B.L.N. & Goleby, B., 2007. New constraints on the seismic structure of West Australia: Evidence for terrane stabilization prior to the assembly of an ancient continent?, *Geology*, **35**, 379–379. doi: 10.1130/G23341A.1

Reading, A.M., Tkalčić, H., Kennett, B.L.N., Johnson, S.P. & Sheppard, S., 2012. Seismic structure of the crust and uppermost mantle of the Capricorn and Paterson Orogens and adjacent cratons, Western Australia, from passive seismic transects, *Precambrian Res.*, **196**, 295—308; doi: 10.1016/j.precamres.2011.07.001

Salmon, M., Kennett, B.L.N., Stern, T. & Aitken, A.R.A., 2013. The Moho in Australia and New Zealand, Tectonophysics, 609, 288–298; doi: 10.1016/j.tecto.2012.07.009

Shibutani, T., Sambridge, M. & Kennett, B., 1996. Genetic algorithm inversion for receiver functions with application to crust and uppermost mantle structure beneath eastern Australia, *Geophys. Res. Lett.*, **23**, 1829–1829. doi: 10.1029/96GL01671

Sippl, C., 2016. Moho geometry along a north–south passive seismic transect through Central Australia. *Tectonophysics*, **676**, 56–69. doi: 10.1016/j.tecto.2016.03.031

Sippl, C., Brisbout, L., Spaggiari, C.V., Gessner, K., Tkalčić, H., Kennett, B.L.N. & Murdie, R., 2017. Crustal structure of a Proterozoic craton boundary: East Albany-Fraser Orogen, Western Australia, imaged with passive seismic and gravity anomaly data, *Precambrian Res.*, **296**, 78–92. doi:10.1016/j.precamres.2017.04.041

Smith, W.H.F. & Wessel P., 1990. Gridding with continuous curvature splines in tension, *Geophysics*, **55**, 293-305. doi: 10.1190/1.1442837

Sun, W. & Kennett, B.L.N. 2016. Receiver structure from teleseisms: auto- and cross-correlation, *Geophys. Res. Lett.*, **43**, 6234–6242, doi:10.1002/2016GL069564

Thompson, D.A., Bastow, A.D., Helffrich, G., Kendall, J.-M., Wookey, J., Snyder, D.B. & Eaton, D.W., 2010. Precambrian crustal evolution: Seismic constraints from the Canadian Shield, *Earth Planet. Sci. Lett.*, **297**, 655–666. doi: 10.1016/j.epsl.2010.07.021

Tian, R., Dentith, M., Murdie, R., Yuan, H. & Gessner, K., 2020. Geophysical Characterisation of Crustal Scale Mineral Systems: A Passive Seismic Experiment Across World-Class Orogenic Gold Deposits, Kalgoorlie Area, Western Australia, *19th International Symposium on Deep Seismic Profiling of the Continents and their Margins*, Perth, Australia

Tkalčić, H., Rawlinson, N., Arroucau, P., Kumar, A. & Kennett, B.L.N., 2011. Multi-step modelling of receiver-based seismic and ambient noise data from WOMBAT array: crustal structure beneath southeast Australia, Geophys. J. Int., 189, 1681-1700. doi: 10.1111/j.1365-246X.2012.05442

Tugume, F., Nyblade, A., Julià, J. & van der Meijde, M., 2013. Precambrian crustal structure in Africa and Arabia: Evidence lacking for secular variation, *Tectonophysics*, **609**, 250–266. doi: 10.1016/j.tecto.2013.04.027

van der Hilst, R., Kennett, B.L.N., Christie, D. & Grant, J., 1994. Project SKIPPY explores the lithosphere and mantle beneath Australia. *Eos Transactions, American Geophysical Union* **75**, 177. doi: 10.1029/94EO00857

Wessel, P. & Smith, W.H.F., 1998. New, improved version of generic mapping tools released, *EOS, Trans. Am. Geophys. Un.*, **79**, 579. doi: 10.1029/98EO00426

Yu, Y., Song, J., Liu, K.H. & Gao, S.S., 2015. Determining crustal structure beneath seismic stations overlying a low-velocity sedimentary layer using receiver functions. *J. Geophys. Res.: Solid Earth*, **120**, 3208-3218 doi: 10.1002/2014JB011610

Yuan, H., 2015. Secular change in Archaean crust formation recorded in Western Australia, *Nature Geoscience*, **8**, 808–813. doi: 10.1038/ngeo2521

Yuan, H. & Bodin, T., 2018. A probabilistic shear wave velocity model of the crust in the central West Australian Craton constrained by transdimensional inversion of ambient noise dispersion. *Tectonics*, **37**, 1994–2012. doi: 10.1029/2017TC004834

Yuan, H., Johnson, S., Dentith, M., Murdie, R., Gessner, K., Korhonen, F. & Bodin, T., 2017. Seismic structure of a late-Archean microcontinent in the middle of the Western Australian Craton. *EGU General Assembly Conference Abstracts* **19**.

Zhao, L., Tyler, I.M., Gorczyk, W., Murdie, R.E., Gessner, K., Lu, Y., Smithies, H., Li, T., Yang, J., Zhan, A., Wan, B., Sun, B. & Yuan, H., 2022. Seismic evidence of two cryptic sutures in Northwestern Australia: Implications for the style of subduction during the Paleoproterozoic assembly of Columbia. *Earth Planet. Sci. Lett.*, **579**, 117342. doi: 10.1016/j.epsl.2021.117342

Zhang, P. & Miller, M.S., 2021. Seismic imaging of the subducted Australian continental margin beneath Timor and the Banda Arc collision zone. *Geophys. Res. Lett.*, **48**, e2020GL089632. doi: 10.1029/2020GL089632

Zhu, L., & Kanamori, H., 2000. Moho depth variation in southern California from teleseismic receiver functions, *J. Geophys. Res.*, **105**, 2969–2980. doi: 10.1029/1999JB900322

Geophys. J. Int.

Refining the Moho across the Australian continent:

Supplementary Information

B.L.N. Kennett[1*], A. Gorbatov[2], H. Yuan[3,4], S. Agrawal[1], R. Murdie[4], M. Doublier[2], C. Eakin[1], M.S. Miller[1], L. Zhao[5], K. Czarnota[2], J.P. O'Donnell[6+], M. Dentith[3], K. Gessner[4].

[1] *Research School of Earth Sciences, The Australian National University, Canberra ACT 2601, Australia*

[2] *Geoscience Australia*

[3] *University of Western Australia*

[4] *Geological Survey of Western Australia*

[5] *Institute of Geology & Geophysics, Chinese Academy of Sciences*

[6] *Geological Survey of South Australia*

[*] *Corresponding author: Brian.Kennett@anu.edu.au*

S1 STATION DISTRIBUTION

Figure S1 displays the full suite of seismic stations that have been deployed across Australia by different agencies up to the end of 2021. The permanent stations and the stations in the Australian Seismometers in Schools network (AUSIS) are identified by name. Temporary stations are linked to the University or agency responsible for the deployment (ANU - Australian National University; GA-EFTF: Geoscience Australia - Exploring for the Future; GSSA: Geological Survey of South Australia, IGGCAS - Institute of Geology & Geophysics, Chinese Academy of Sciences, UTas - University of Tasmania, UWA - University of Western Australia). The SWAN experiment in southwestern Australia is a multi-agency effort involving the Geological Survey of Western Australia, the Australian National University, the University of Western Australia and Macquarie University supported by an Australian Research Council Linkage Grant. AuScope is the Australian National Earth Sciences Infrastructure Project enabled by the National Collaborative Research Infrastructure Strategy (NCRIS) of the Australian Government.

+ Now at Geological Survey of Western Australia

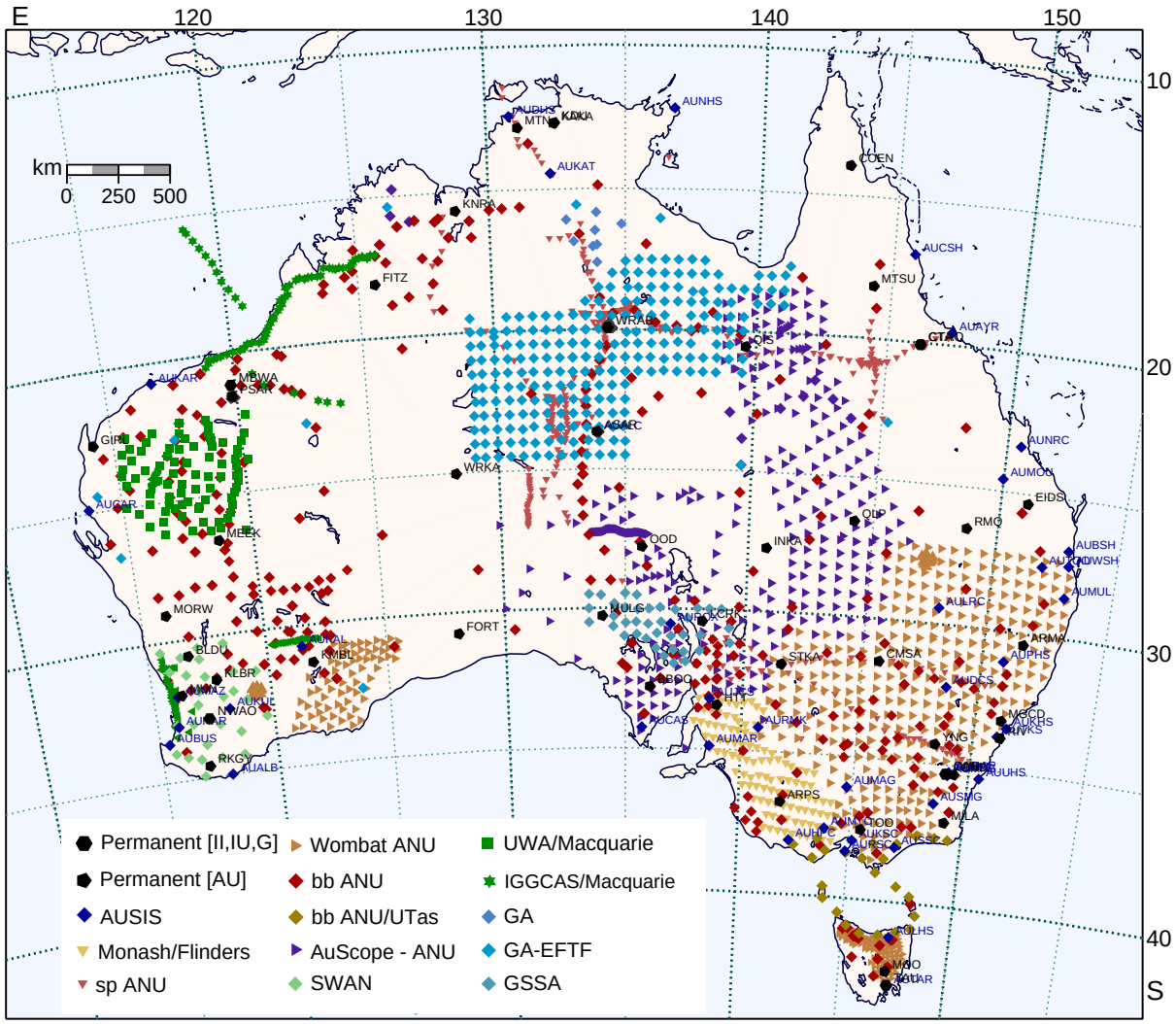

Figure S1. Seismic station distribution across Australia to end 2022.

The following tables provide details of the full range of networks whose data has been used in the construction of the current Moho surface. For global networks only the number of stations on the Australian continent is provided.

We have divided the networks by the primary style of analysis that has been employed with the data from teleseismic events. Receiver function studies include waveform inversion, *H*-*k* stacking, and interpretation of migrated data. Autocorrelation studies have used both continuous data and the same section of the teleseismic arrivals as used for receiver function anlysis.

Permanent station data can be obtained from Incorporated Research Institutions for Seismology (IRIS) Data Services (http://ds.iris.edu/ds/) and the data from temporary stations from the AusPass repository (http://auspass.edu.au/).

Table 1. Networks used for Receiver Function analysis

Code	Name	Stations	Begin	End	doi
II	GSN-IRIS/IDA	2	ongoing		10.7914/SN/II
IU	GSN-IRIS/USGS	3	ongoing		10.7914/SN/IU
G	GEOSCOPE	1	1987	ongoing	10.18715/GEOSCOPE.G
AU	ANSN	50	1994	ongoing	10.26186/144675
S1	AUSIS	49	2011-09-01	ongoing	10.7914/SN/S1
7E	KIMBA98	6	1998-05-22	1998-07-25	10.7914/SN/7E_1998
7D	KIMBA97	7	1997-07-21	1997-10-14	10.7914/SN/7D_1997
7B	SKIPPY	37	1993-05-03	1995-08-10	10.7914/SN/7B_1993
7G	WA CRATON	25	2000-07-11	2001-07-13	10.7914/SN/7G_2000
1P	BASS	24	2011-05-22	2012-12-31	10.7914/SN/1P_2011
S1	AUSIS	49	2011-09-01	ongoing	10.7914/SN/S1
7I	TASMAL	24	2003-05-01	2005-11-17	10.7914/SN/7I_2003
7J	CAPRAL	25	2005-10-20	2007-05-30	10.7914/SN/7J_2005
YS	BANDA	11	2016-11-21	2019-08-20	10.7914/SN/YS_2014
8K	COPA-HPS	29	2014-10-12	2015-10-16	10.7914/SN/8K_2014
7M	COPA	80	2014-02-24	2018-09-04	10.7914/SN/7M_2014
1E	SQLD SPIRAL	16	2013-11-12	2014-11-13	10.7914/SN/1E_2013
1K	ALFREX	70	2013-11-06	2015-09-14	10.7914/SN/1K_2013
1P	BASS	24	2011-05-22	2012-12-31	10.7914/SN/1P_2011
1F	CURNAMONA	34	2009-03-24	2009-11-05	10.7914/SN/1F_2009
6F	BILBY	25	2008-08-27	2011-05-24	10.7914/SN/6F_2008
1G	GAWLER	35	2008-07-01	2009-04-03	10.7914/SN/1G_2008
7K	SOC	21	2007-02-14	2008-08-14	10.7914/SN/7K_2007
7J	CAPRAL	25	2005-10-20	2007-05-30	10.7914/SN/7J_2005
7I	TASMAL	24	2003-05-01	2005-11-17	10.7914/SN/7I_2003
7G	WA CRATON	25	2000-07-11	2001-07-13	10.7914/SN/7G_2000
7H	TIGGER BB	17	2001-10-03	2002-08-17	10.7914/SN/7H_2002
6K	AUSARRAY SA	38	2020-10-14	2022-06-11	10.7914/SN/6K_2020
2P	SWAN	27	2020-08-13	2023	10.7914/SN/2P_2020
8M	MULGA	5	2016-06-06	2016-09-19	10.7914/SN/8M_2016
6C	WA SPIRAL	16	2015-02-15	2016-01-03	10.7914/SN/6C_2015
3O	AKIMBA19	8	2019-05-09	2020-05-22	10.7914/SN/3O_2019
3G	MARLA LINE	66	2018-04-21	2019-08-04	10.7914/SN/3G_2018
5G	LAKE EYRE BASIN	40	2018-10-16	2022-06-14	10.7914/SN/5G_2018
6K	AUSARRAY SA	38	2020-10-14	2022-06-11	10.7914/SN/6K_2020
OA	EFTF/GA	100	2017-09-13	2021-04-01	10.11636/135284
4N	CWAS	60	2017	2022	10.7914/SN/4N_2017
2O	BEETALOO	8	2021-09	2025	10.7914/SN/2O_2019

Table 2. Networks used for Autocorrelation Analysis

Code	Name	Stations	Begin	End	doi
7M	MALT LF98	40	1998-05-04	1998-09-23	10.7914/SN/7M_1998
7O	MALT AF00	40	2000-01-16	2000-07-08	10.7914/SN/7O_2000
7N	MALT MB99	40	1999-03-14	1999-07-25	10.7914/SN/7N_1999
4J	AQ3	52	2014-05-20	2016-02-09	10.7914/SN/4J_2014
8J	SQEAL	98	2012-11-19	2014-10-12	10.7914/SN/8J_2012
7L	EAL3	44	2011-11-09	2013-07-07	10.7914/SN/7L_2011
1H	EAL2	52	2010-05-10	2011-03-22	10.7914/SN/1H_2010
4H	EAL1	44	2009-06-02	2010-02-26	10.7914/SN/4H_2009
ZR	MINQ	53	2009-06-16	2011-04-01	10.7914/SN/ZR_2009
7U	SEAL3	57	2007-11-14	2009-02-14	10.7914/SN/7U_2007
7T	SEAL2	31	2007-02-11	2007-11-19	10.7914/SN/7T_2007
7S	SETA	41	2006-10-02	2007-08-26	10.7914/SN/7S_2006
7R	EVA	50	2005-07-19	2006-05-23	10.7914/SN/7R_2005
7Q	SEAL	20	2004-11-03	2005-04-09	10.7914/SN/7Q_2004
7I	TASMAL	24	2003-05-01	2005-11-17	10.7914/SN/7I_2003
7H	TIGGER BB	17	2001-10-03	2002-08-17	10.7914/SN/7H_2002
1K	ALFREX	70	2013-11-06	2015-09-14	10.7914/SN/1K_2013
3G	MARLA LINE	66	2018-04-21	2019-08-04	10.7914/SN/3G_2018
5J	ASR	12	2017-04-23	2019-02-28	10.7914/SN/5J_2018
1Q	AQT	87	2015-11-28	2017-10-24	10.7914/SN/1Q_2016

S2 MOHO ESTIMATES

Figures S2–S4 show the distribution of the Moho estimates from the different classes of seismological techniques employed to produce the Moho surface shown in Figure 3 of the main paper.

The full set of refraction information is displayed in Figure S2 with receiver locations and shotpoints. Figure S2 also shows the control points extracted for use in the Moho compilation, designed to provide directional control and represent the distance span associated with the Moho value (rather than provide just a point measurement). Refraction results provide direct depth information on the transition from crust to mantle though they are dependent on the assumptions made in the interpretation. However, Moho depth estimates from early experiments were assigned to a single point, even when the interpretation covered a broad area, and may not actually be representative of the local conditions at the assigned point.

We also display in Figure S2 a few Moho estimates that were extracted from analysis of tomographic results in central Australia and northern Tasmania. These are indicated with triangular symbols.

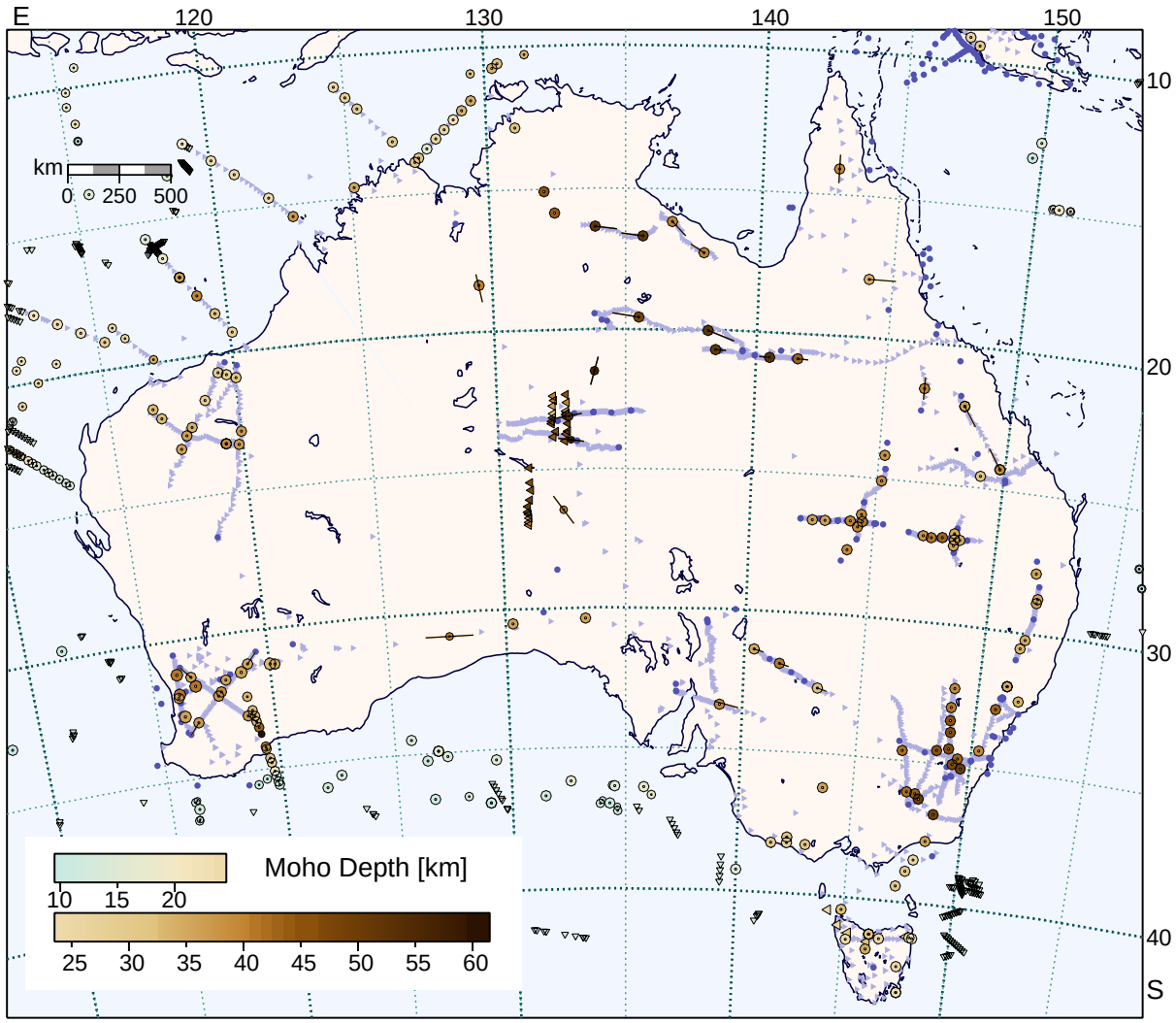

Figure S2. Refraction and marine reflection results. Shots are shown with purple circles and stations with violet triangles. The control points used in the Moho compilation are shown with circles, the symbol size indicates reliability. Results from tomography in central Australia and northern Tasmania are also included, shown with triangular symbols.

Figure S3 shows the full suite of receiver function results, with many analyses using waveform inversion and *H*-*k* stacking to provide direct depth estimates. There are hidden dependencies on the style of model employed, and for stacking on the assumed average P wavespeed in the crust. The stacking methods for receiver functions tend not to work too well where there is a transition zone at the base of the crust rather than a sharp interface between crust and mantle. Problems can also arise in areas with thick sediment where shallow multiples obscure the main Moho arrival. The 'other' category for receiver functions includes joint inversion with surface waves, stacking with migration and situations where multiples from the Moho are weak, as in the Lake Eyre Basin, forcing interpretation to be based on the Moho arrival alone, with conversion from time to depth.

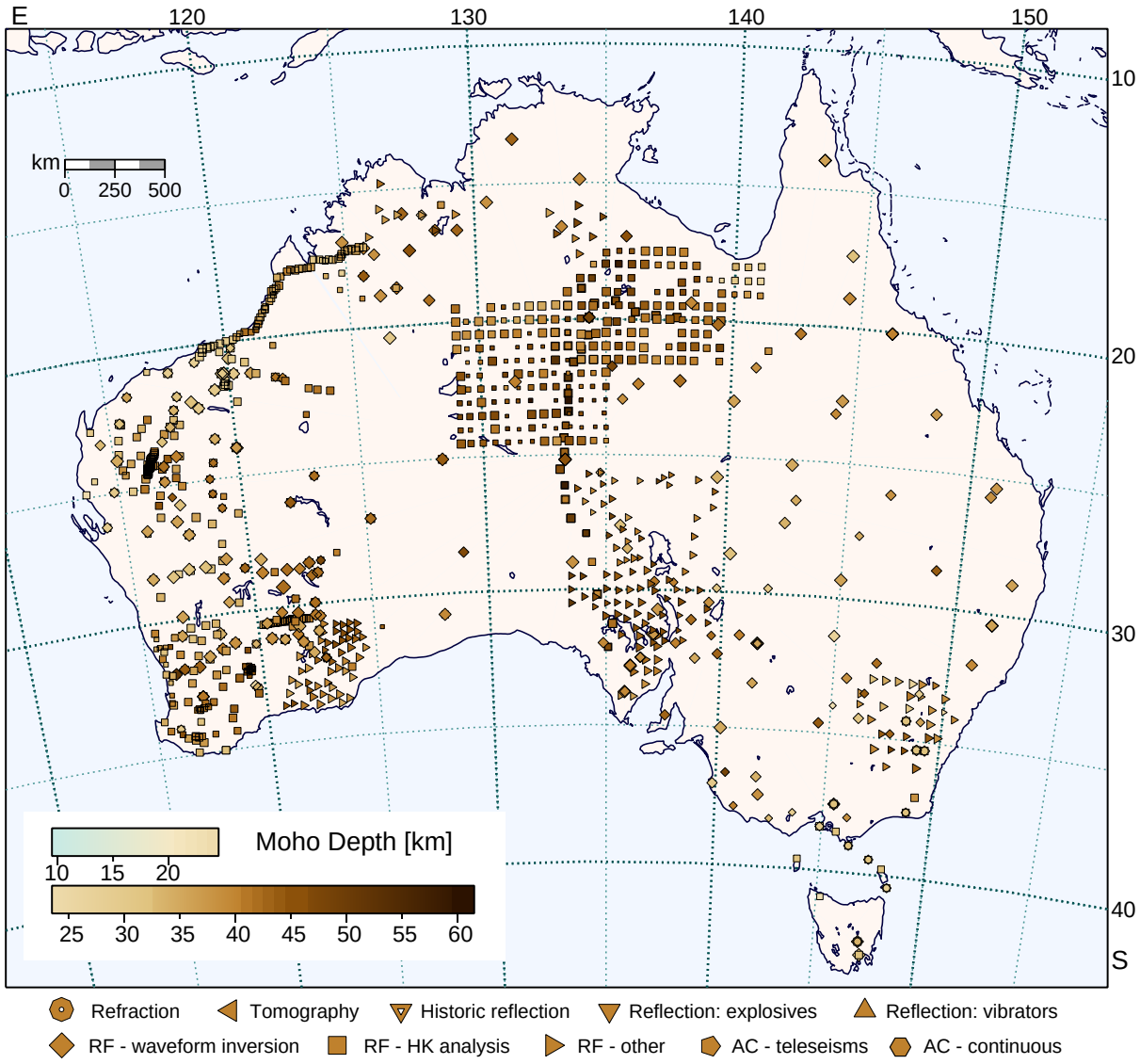

Figure S3. Receiver function Moho estimates and results from tomography. Symbol size indicates reliability.

Figure S4 displays the Moho estimates extracted from the analysis of full-crustal reflection profiling together with those extracted from P wave reflectivity constructed from autocorrelation studies. We display results from both continuous data and from teleseismic P arrivals using the same portion of the records exploited in receiver function analysis. In each case, the primary estimate for the Moho is terms of the time of reflection for P waves from the base of the crust and has to be converted to depth. Sedimentary corrections are applied to these reflection results based on the shallow part of the section. The depth conversions are cross checked against nearby receiver function results to ensure adequate calibration. Autocorrelation methods can cope with complex near-surface conditions that cause difficulties for Ps receiver functions relying on conversion from teleseismic P to local S waves.

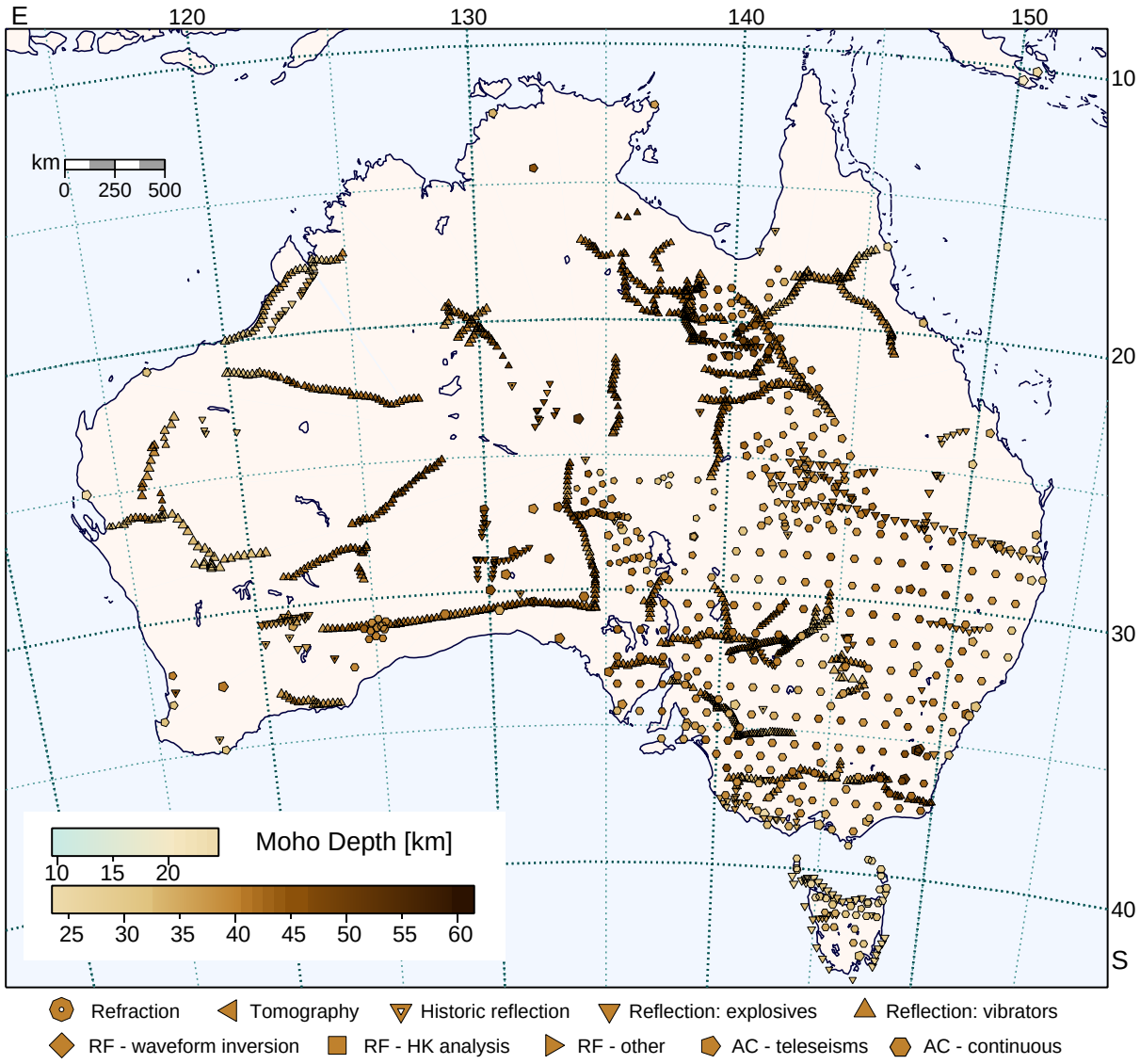

Figure S4. Moho results from full-crustal reflection profiling and autocorrelation studies, where conversion from time to depth is required. Symbol size indicates reliability.

S3 COMPARATOR STUDIES

In Figure S5 we display the suite of Moho estimates constructed by Qashqai et al. (2019) using waveform inversion of the autocorrelation of teleseismic arrivals, superimposed on the new Moho surface. These results from Qashqai et al. (2019) employ a three layer crustal model with wavespeed discontinuities, so can have some difficulties where the base of the crust is gradational. The inversion scheme of Qashqai et al. (2019) exploits just vertical component records and so is able to extract results from some older data sets in southeastern Australia that did not have three-component recording. This set of results has the merit of providing independent control on the Moho distribution exploiting a wide range of temporary and permanent stations. In general there is a good correspondence with the

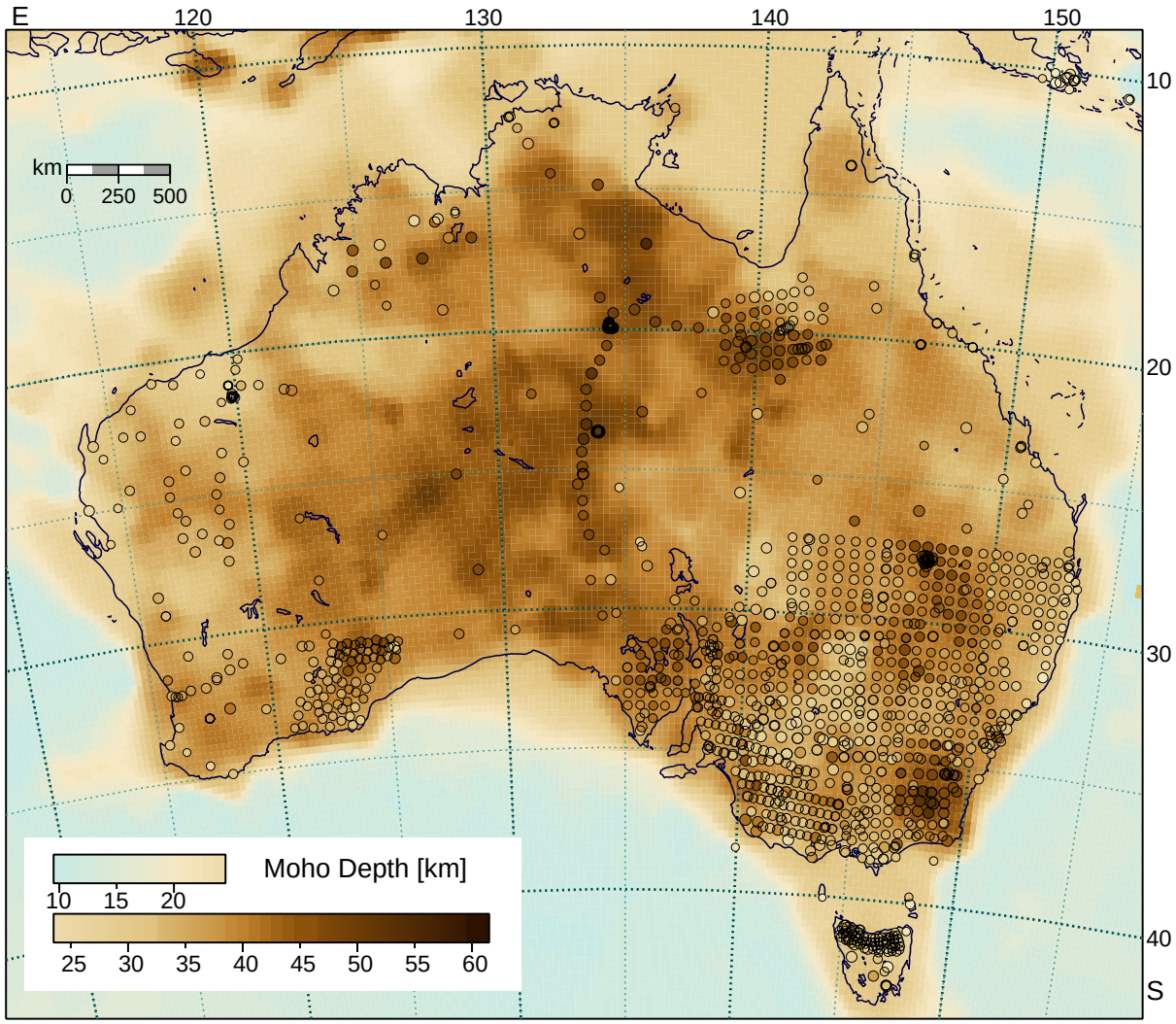

Figure S5. Distribution of Moho estimates from the work of Qashqai et al. (2019) using waveform inversion of station autocorrelations from teleseismic P arrivals, with a three-layer crust, superimposed on the new Moho surface. The stations are marked with circles and symbol size indicates reliability.

other classes of results, though the assumption of a strong contrast between crust and mantle tends to produce shallower results where there is actually a gradational transition.

A second independent study is provided by the work of Birkey et al. (2021), who have constructed teleseismic receiver function stacks for both incident S and P waves to look at the full range of lithospheric discontinuities beneath stations. They present Moho results for 35 stations and these are summarised in Figure S6 as differences from the Moho surface constructed in this work. We show both the Ps and Sp results, where available. For Ps (incident teleseismic P) we show the results as circles, and for Sp (incident teleseismic S) as diamonds. The size of symbols is again scaled by the reliability of the estimates, in this case the inverse of the error range for the results.

For the majority of stations the Ps estimates lie close to the Moho results derived by other means,

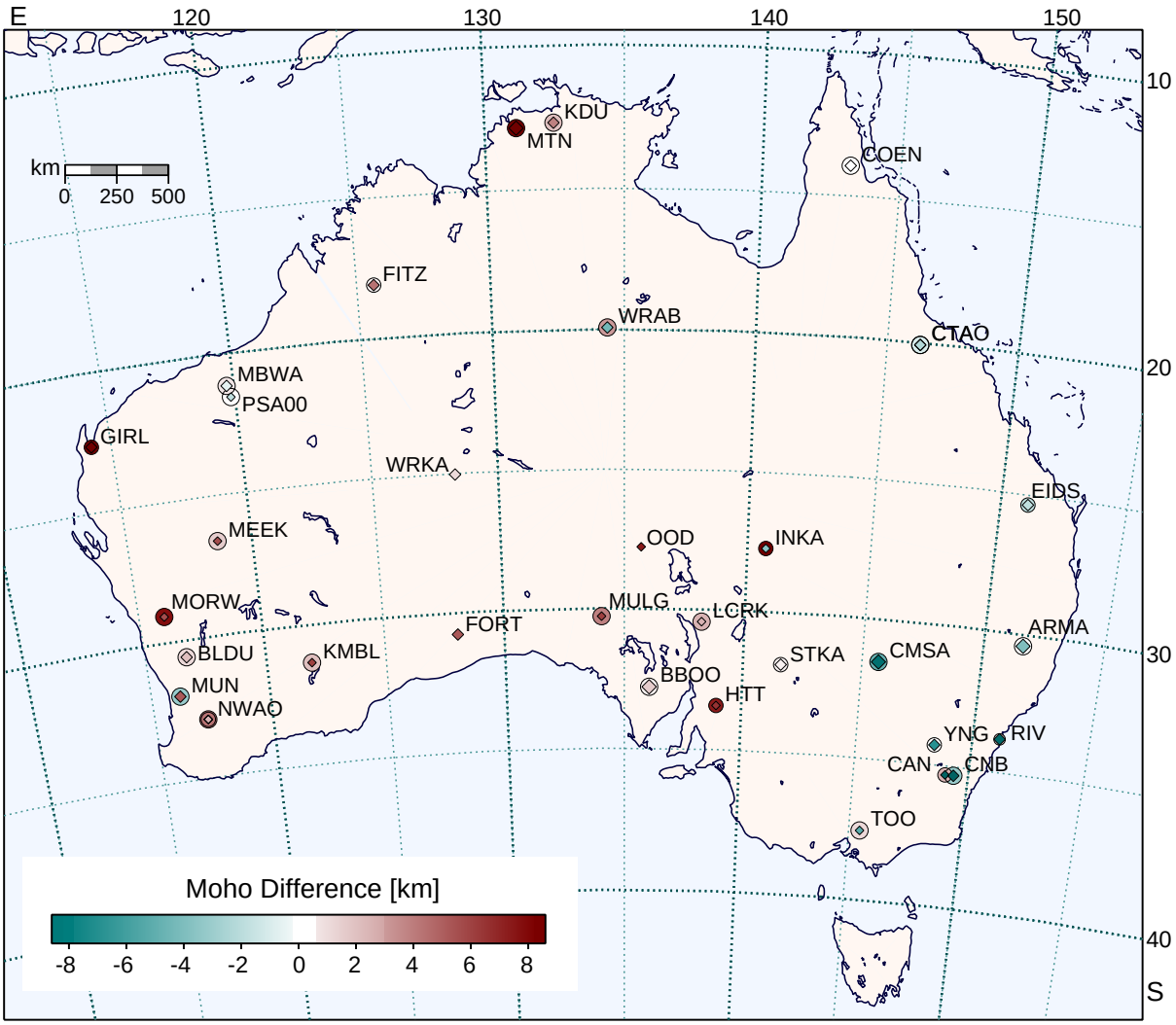

Figure S6. Comparison of stacked receiver function Moho estimates from Birkey et al. (2021) with the new Moho surface. Ps results are shown with circles and Sp with diamonds. Negative differences indicate shallower Moho from the RF stacks, and positive deeper. Symbol size indicates reliability, based on the estimates of likely error in depth.

but there are several stations (GIRL, MORW, MTN, HTT) where the estimates from Birkey et al. (20121) are considerably deeper from those from other analyses (including Qashqai et al., 2019). There are more differences for the results from incident S, but the frequencies employed are lower and so intrinsic resolution is less. For several stations in the east, the Sp results suggest the presence of a discontinuity at a shallower depth than the base of the crust indicated from other methods. In areas where there is a gradational transition in properties between crust and mantle, an apparent discontinuity can be produced at the top of the gradient zone when interrogated by lower frequency waves.

S4 MOHO DEPTH BY PROVINCE

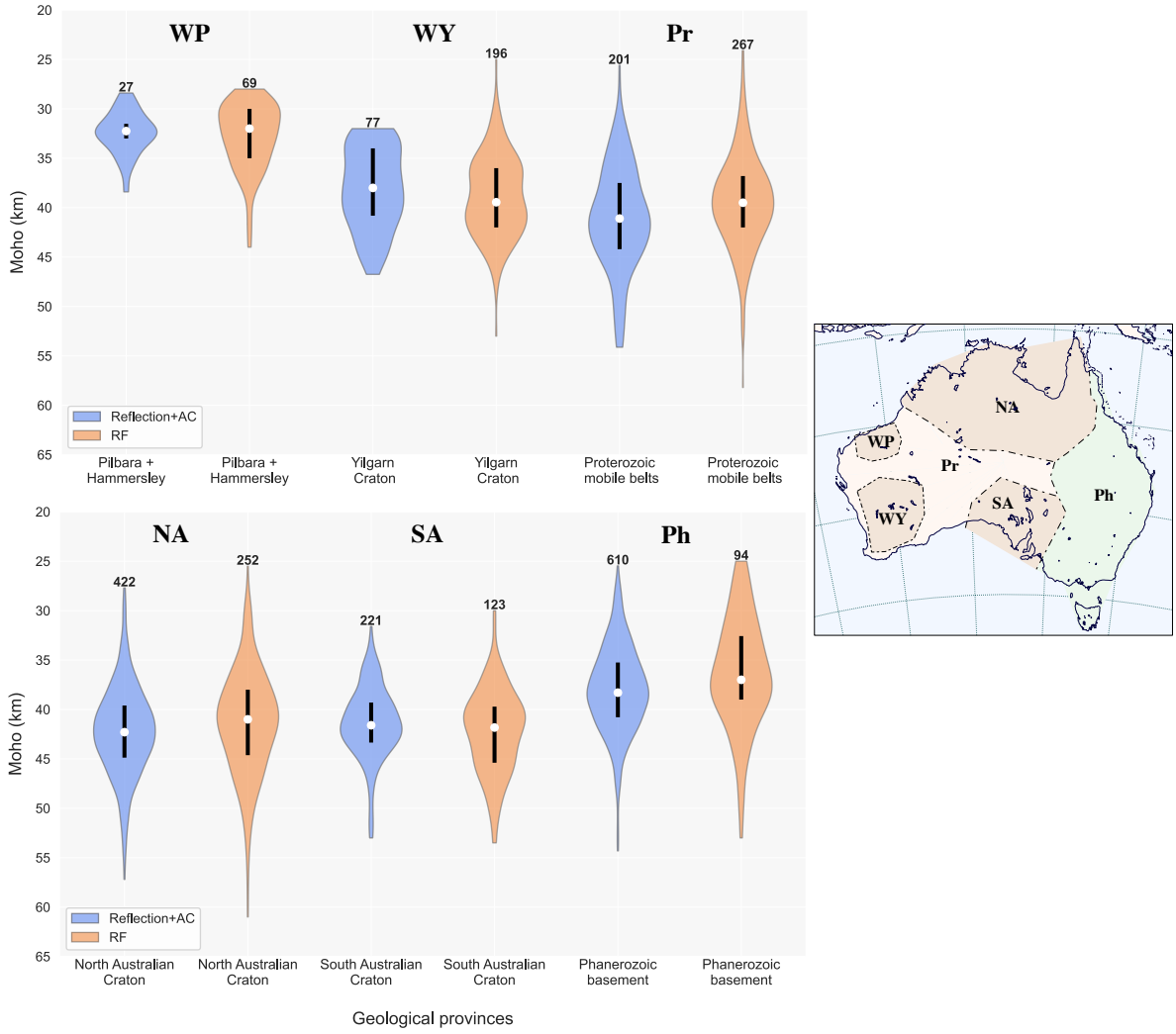

Figure S7. Moho depth distribution for continental Australia expressed as violin plots. Australia is divided into six provinces based on age and geological history (as in insert map). Each violin plot displays the full distribution of the Moho estimates in depth with the median shown as a white circle and the interval between the second and third quartiles with a black bar. Separate displays are shown for receiver function results and for reflection profiles plus autocorrelation studies, where there is a conversion from time to depth.

In Figure S7 we consider the same set of six regional elements as in Figure 7 of the main paper, but now separate the receiver function results from those from reflection profiles and autocorrelation studies, where depth conversion is needed. There is a very good correspondence between the different types of results, though the receiver function estimates tend to have longer tails, both shallower and deeper. As a result we can have confidence in the distributions displayed using the full suite of results.

S5 MOHO DATA SOURCES

We provide below a list of the published works that have been used in the assembly of the Moho estimates used in this work. These are supplemented by additional studies on recent data.

Seismic reflection data acquired with government funding up to the end of 2015 are displayed in a uniform format in Kennett et al. (2016), which also provides references for the interpretation of the profiles. More recent data is available through the data portal for the Exploring the Future project at Geoscience Australia (https://portal.ga.gov.au/persona/eftf) under Onshore Seismic Surveys.

Publications:

Aitken A.R.A., 2010. Moho geometry gravity inversion experiment (MoGGIE): A refined model of the Australian Moho and its tectonic and isostatic implications. *Earth Planet. Sci. Lett.*, **297**, 71–83. doi: 10.1016/j.epsl.2010.06.004

Aitken, A.R.A., Salmon, M.L., Kennett, B.L.N. 2013. Australia's Moho: A test of the usefulness of gravity modelling for the determination of Moho depth, *Tectonophysics*, **609**, 468–479; doi: 10.1016/j.tecto.2012.06.049

Balfour, N.J., Salmon M., Sambridge, M., 2014. The Australian Seismometers in Schools network: education, outreach, research, and monitoring, *Seism. Res. Lett.*, **85**, 1063–1068; doi: 10.1785/0220140025

Bello M., Cornwell D.G., Rawlinson N., Reading A.M., Likkason O.K., 2021. Crustal structure of southeast Australia from teleseismic receiver functions, *Solid Earth*, **12**, 463–481; doi: 10.5194/se-12-463-2021

Birkey, A., Ford, H. A., Dabney, P., Goldhagen, G., 2021. The lithospheric architecture of Australia from seismic receiver functions. *J. Geophys. Res.: Solid Earth*, **126**, e2020JB020999. doi: 10.1029/2020JB020999

Bowman, J.R., Kennett, B.L.N., 1991. Propagation of *Lg* waves in the North Australian craton: influence of crustal velocity gradients, *Bull. Seism. Soc. Am.*, **81**, 592–610.

Clitheroe, G., Gudmundsson, O., Kennett, B.L.N., 2000. The crustal thickness of Australia. J. Geophys. Res., 105, 13 697–13 713; doi: 10.1029/1999JB900317

Collins, C.D.N., 1991. The nature of the crust-mantle boundary under Australia from seismic evidence. *The Australian Lithosphere*, edited by B.J. Drummond, Spec. Publ., Geol. Soc. Aust., **17**, 67–80.

Collins C.D.N., Drummond B.J., Nicoll M.G., 2003. Moho depth patterns in the Australian continent. 121–128, in *The Evolution and Dynamics of the Australian Plate*, Ed. D. Müller and R. Hillis. Geol. Soc. of Australia Special Publication **22** and Geol. Soc. of America Special Paper **372**. doi: 10.1130/0-8137-2372-8.121

Czarnota K., Hoggard M. J., White N., Winterbourne J., 2013. Spatial and temporal patterns of Cenozoic dynamic topography around Australia, *Geochem. Geophys. Geosyst.*, *14*, 634—658; doi:10.1029/2012GC004392

Dentith, M., Yuan, H., Murdie, R.E., Pina-Varas, P., Johnson, S.P., Gessner, K., Korhonen, F.J., 2018. Improved interpretation of deep seismic reflection data in areas of complex geology through integration with passive seismic data sets. *J. Geophys. Res.: Solid Earth*, **123**, 10 810-10 830; doi: 10.1029/2018JB015795

Dooley, J.C., Moss, F.J., 1988. Deep crustal reflections in Australia 1957-1973 – II. Crustal models. *Geophys. J. R. Astr. Soc.*, **293**, 239–249. doi: 10.1111/j.1365-246X.1988.tb01999.x

Doublier, M.P., Johnson, S.P., Gessner, K., Howard, H., Chopping, R., Smithies, R.H., Martin, D.McB., Kelsey, D.E., Haines, P.W., Hickman, A., Czarnota, K., Southby, C., Champion, D.C., Huston, D.L., Calvert, A.J., Kohanpour, F., Moro, P., Costelloe, R., Fomin, T. & Kennett, B.L.N., 2020. Basement architecture from the Pilbara Craton to the Aileron Province: new insights from deep seismic reflection line 18GA-KB1. In: Czarnota, K., Roach, I., Abbott, S., Haynes, M., Kositcin, N., Ray, A., Slatter, E. (eds.), *Exploring for the Future: Extended Abstracts*, Geoscience Australia, Canberra.

Doublier, M.P., Gessner, K., Johnson, S.P., Kelsey, D.E., Haines, P.W., Howard, H.M., Chopping, R., Smithies, R.H., Hickman, A.H., Martin, D.McB., Southby, C., Champion, D.C., Huston, D.L., Calvert, A.J., Gorczyk, W., Kohanpour, F., Moro, P., Costelloe, R., Fomin, T., Yuan, H. & Kennett, B.L.N. 2022, Interpretation of the basement component of seismic line 18GA-KB1, in Carr, L.K., Southby, C., Edwards, D.S., Anderson, J.R. & MacFarlane, S.K. (eds) *Exploring for the Future: Canning Basin: Kidson Seismic survey (18GA-KB1) and geological interpretation*. Geoscience Australia Record 2022/16, 35–48

Dutch, R.A., Pawley, M.J. & Wise, T.W. (editors), 2015. *What lies beneath the Western Gawler Craton? 13GA-EG1 Seismic and Magnetotelluric Workshop 2015 — extended abstracts*: Department of State Development, South Australia, Report Book 2015/00029, 84p

Eakin, C.M., 2019. Seismicity, Minerals, and Craton margins: The Lake Eyre Basin Seismic Deployment. *ASEG Extended Abstracts*, **1**, 1–2; doi:10.1080/22020586.2019.12072989

Fauzi, M.F., Anggraini, A., Riyanto, A., Ngadmanto, D., Suryanto, W., 2021. Crustal thickness estimation in Indonesia using receiver function method, *IOP Conf. Series: Earth and Environmental Science*, **873**, 012086; doi:10.1088/1755-1315/873/1/012086

Finlayson, D. M., 1993. Crustal architecture across the Phanerozoic Australia along the Eromanga-Brisbane Geoscience Transect: evolution and analogues. *Tectonophysics*, **219**, 191–211; doi: 10.1016/0040-1951(93)90296-V

Finlayson, D.M., 2010. A Chronicle of Deep Seismic Profiling across the Australian Continent and its Margins, 1946-2006, D.M. Finlayson, Canberra, pp. 255 (available from: doug.finlayson@netspeed.com.au).

Fishwick S., Kennett B.L.N., Reading A.M., 2005, Contrasts in lithospheric structure within the Australian Craton. *Earth Planet. Sci. Lett.*, **231**, 163—176; doi: 10.1016/j.epsl.2005.01.009

Fishwick, S., Heintz, M., Kennett, B.L.N., Reading, A.M., Yoshizawa, K., 2008. Steps in lithospheric thickness within eastern Australia, evidence from surface wave tomography. *Tectonics*, **27**, TC0049; doi:10.129/2007TC002116.

Fishwick S., Reading A.M., 2008, Anomalous lithosphere beneath the Proterozoic of western and central Australia: A record of continental collision and intraplate deformation? *Precambrian Res.*, **166**, 111–121. doi:10.1016/j.precamres.2007.04.026

Fontaine, F., Tkalčić, H., Kennett, B.L.N., 2013a, Imaging crustal structure variation across southeastern Australia, *Tectonophysics*, **582**, 112–125; doi: 10.1016/j.tecto.2012.09.031

Fontaine, F., Tkalčić, H., Kennett, B., 2013b, Crustal complexity in the Lachlan Orogen revealed from teleseismic receiver functions, *Austral. J. Earth Sci.*, **60**, 413–430; doi:10.180/08120099.2013.787646

Ford, H.A., Fischer, K.M., Abt, D.L., Rychert, C.A., Elkins-Tanton, L.T., 2010. The lithosphere-asthenosphere boundary and cratonic lithospheric layering beneath Australia from *Sp* wave imaging, *Earth Planet. Sci. Lett.*, **300**, 299–310. doi: 10.1016/j.epsl.2010.10.007

Galybin, K.A., 2006. *P-wave Velocity Model for the Southwest of the Yilgarn Craton, Western Australia and its Relation to the Local Geology and Seismicity*, Ph.D. thesis, University of Western Australia.

Goleby, B.R., Shaw, R.S., Wright, C., Kennett, B.L.N., Lambeck, K., 1989. Geophysical evidence for 'thick-skinned' crustal deformation in central Australia, *Nature*, **337**, 325-330.

Goncharov, A., Deighton, I., Tischer, M., Collins, C., 2007. Moho depth in Australia: where, how and what for? *ASEG Extended Abstracts, Perth, Western Australia*.

Gorbatov, A., Kennett, B.L.N., Saygin, E., 2013. Crustal properties from seismic station autocorrelograms, *Geophys. J. Int.*, **192**, 861–870; doi: 10.1093/gji/ggs064

Gorbatov A., Medlin A., Kennett B.L.N., Doublier M.P., Czarnota K., Fomin T., Henson P., 2020. Moho variations in northern Australia. In: Czarnota, K., Roach, I., Abbott, S., Haynes, M., Kositcin, N., Ray, A., Slatter, E. (eds.), *Exploring for the Future: Extended Abstracts*, Geoscience Australia, Canberra, 1–4.

Kennett, B.L.N., Fishwick, S., Reading, A.M., Rawlinson, N., 2004. Contrasts in mantle structure beneath Australia: relation to Tasman Lines? *Austral. J. Earth Sci.*, **51**, 563–569. doi: 10.1111/j.1400-0952.2004.01075.x

Kennett, B.L.N., Salmon, M., Saygin E., AusMoho Working Group, 2011, AusMoho: the variation of Moho depth in Australia. *Geophys. J. Int.*, **187**, 946–958; doi: 10.1111/j.1365-246x.2011.05194.x

Kennett, B.L.N., Saygin, E., 2015. The nature of the Moho in Australia from reflection profiling: A review, *GeoResJ*, **5**, 74–91; doi: 10.1016/j.grj.2015.02.001

Kennett, B.L.N., Saygin, E., Salmon, M., 2015. Stacking autocorrelograms to map Moho depth with high spatial resolution in southeastern Australia, *Geophys. Res. Lett.*, **42**, 3839–3846; doi: 10.1002/2015GL065345

Kennett, B.L.N., Saygin, E., Fomin, T., Blewett, R.S., 2016, *Deep Crustal Seismic Reflection Profiling Australia 1978–2015*, ANU Press, Canberra; doi: 10.22459/dcsrp.11.2016

Kennett, B.L.N., Sippl, C., 2018. Lithospheric discontinuities in central Australia, *Tectonophysics*, **744**, 10—22; doi: 10.1016/j.tecto.2018.06.008

Kennett, B.L.N., 2019. Areal parameter estimates from multiple datasets. *Proc. R. Soc. A*, **475**, 20190352; doi: 10.1098/rspa.2019.0352

Kennett B.L.N., Liang S., 2021. The transition from the Thomson Orogen to the North Australian Craton from seismic data. Australian Journal of Earth Sciences, 68, 628-640; doi: 10.1080/08120099.2021.1837955

Korsch R.J., Goleby B.R., Leven J.H., Drummond B.J., 1998. Crustal architecture of central Australia based on deep seismic reflection profiling, *Tectonophysics*, **288**, 57—69; doi: 10.1016/S0040-1951(97)00283-7

Korsch, R., Koscitin, N., 2010. GOMA (Gawler Craton-Officer Basin-Musgrave Province-Amadeus Basin) seismic and MT workshop 2010 Extended Abstracts, Geoscience Australia Record 2010/039.

Korsch, R., Blewett, R.S., Close, D.F., Scrimgeour, I.R., Huston, D.L., Kositcin, N., Whelan, J.A., Carr, L.K., Duan, J., 2011. Geological interpretation and geodynamic implications of the deep seismic reflection and MT line 09GA-GA1: Georgina Basin-Arunta Region. In *Northern Territory Geological Survey Record 2011-003*.

Lambeck, K., Burgess, G., Shaw, R.D., 1988. Teleseismic travel-time anomalies and deep crustal structure in central Australia, *Geophys. J. R. Astr. Soc.*, **94**, 105–124; doi: 10.1111/j.1365-246X.1988.tb03431.x

Liang S., Kennett B.L.N., 2020. Passive seismic imaging of a craton edge – Central Australia, *Tectonophysics*, **797**, 228662; doi: 10.1016/j.tecto.2020.228662

McQueen, H.W.S., Lambeck, K., 1996. Determination of crustal structure in central Australia by inversion of traveltime residuals, *Geophys. J. Int.*, **126**, 645–662; doi: 10.1111/j.1365-246X.1996.tb04696.x

Moss, F.J., Dooley, J.C. 1988. Deep crustal reflection recordings in Australia 1957-1973 – I. Data acquisition and presentation, *Geophys. J. R. Astr. Soc.*, **293**, 229–238. doi: 10.1111/j.1365-246X.1988.tb01998.x

Murdie, R., Yuan, H., Dentith, M.C. & Lin, X., 2020. A passive seismic experiment in the Perth Basin, Western Australia. *Geological Survey of Western Australia, Report 208*. doi: 10.1080/14432471.2020.1828423

Murdie, R.E., Yuan, H., 2021. Western Australian Moho, 2021, in *Accelerated Geoscience Program: extended abstracts:*, Geological Survey of Western Australia, Record 2021/4, 27–29.

Qashqai, T.M., Saygin E., Kennett B.L.N. 2019. Crustal imaging with Bayesian inversion of teleseismic P-wave coda autocorrelation, *J. Geophys. Res.: Solid Earth*, **124**, 5888–5906; doi: 10.1029/2018JB017055

Rawlinson, N., Tkalčić, H., Reading, A.M., 2010. Structure of the Tasmanian lithosphere from 3D seismic tomography, *Austral. J. Earth Sci.*, **57**, 381–394. doi: 10.1080/08120099.2010.481325

Reading, A.M., Kennett, B.L.N., Dentith, M.C. 2003. The seismic structure of the Yilgarn Craton, Western Australia, *Austral. J. Earth Sci.*, **50**, 427–438; doi: 10.1046/j.1440-0952.2003.01000.x

Reading, A.M., Kennett, B.L.N., 2003. Lithospheric structure of the Pilbara Craton, Capricorn Orogen and northern Yilgarn Craton, Western Australia, from teleseismic receiver functions, *Austral. J. Earth Sci.*, **50**, 439–445; doi: 10.1046/j.1440-0952.2003.01003.x

Reading, A.M., Kennett, B.L.N., Goleby, B., 2007. New constraints on the seismic structure of West Australia: Evidence for terrane stabilization prior to the assembly of an ancient continent? *Geology*, **35**, 379–379; doi: 10.1130/G23341A.1

Reading, A.M., Tkalčić, H., Kennett, B.L.N., Johnson, S.P., Sheppard, S., 2012. Seismic structure of the crust and uppermost mantle of the Capricorn and Paterson Orogens and adjacent cratons, Western Australia, from passive seismic experiments. *Precambrian Res.*, **196–197**, 295–308. doi:10.1016/j.precamres.2011.07.001.

Salmon, M., Kennett, B.L.N., Stern, T., Aitken, A.R.A., 2013. The Moho in Australia and New Zealand, Tectonophysics, 609, 288–298; doi: 10.1016/j.tecto.2012.07.009

Saygin, E., 2007. *Seismic Receiver and Noise Correlation Based Studies in Australia*, Ph.D. Thesis, Australian National University.

Shibutani, T., Sambridge, M., Kennett, B., 1996. Genetic algorithm inversion for receiver functions with application to crust and uppermost mantle structure beneath eastern Australia. *Geophys. Res. Lett.*, **23**, 1829–1829; doi: 10.1029/96GL01671

Sippl, C., 2016. Moho geometry along a north–south passive seismic transect through Central Australia. *Tectonophysics*, **676**, 56–69; doi: 10.1016/j.tecto.2016.03.031

Sippl, C., Brisbout, L., Spaggiari, C.V., Gessner, K., Tkalčić, H., Kennett, B.L.N., Murdie, R., 2017. Crustal structure of a Proterozoic craton boundary: East Albany-Fraser Orogen, Western Australia, imaged with passive seismic and gravity anomaly data, *Precambrian Res.*, **296**, 78–92; doi:10.1016/j.precamres.2017.04.041

Tian, R., Dentith, M., Murdie, R., Yuan, H. & Gessner, K., 2020. Geophysical Characterisation of Crustal Scale Mineral Systems: A Passive Seismic Experiment Across World-Class Orogenic Gold Deposits, Kalgoorlie Area, Western Australia, *19th International Symposium on Deep Seismic Profiling of the Continents and their Margins*, Perth, Australia

Tkalčić, H., Rawlinson, N., Arroucau, P., Kumar, A., Kennett, B.L.N., 2011. Multi-step modelling of receiver-based seismic and ambient noise data from WOMBAT array: crustal structure beneath southeast Australia, *Geophys. J. Int.*, **189**, 1681-1700; doi: 10.1111/j.1365-246X.2012.05442.x

Yuan, H., 2015, Secular change in Archaean crust formation recorded in Western Australia, *Nature Geoscience*, **8**, 808–813; doi: 10.1038/ngeo2521

Zhao, L., Tyler, I.M., Gorczyk, W., Murdie, R.E., Gessner, K., Lu, Y., Smithies, H., Li, T., Yang, J., Zhan, A., Wan, B., Sun, B., Yuan, H., 2022. Seismic evidence of two cryptic sutures in Northwestern Australia: Implications for the style of subduction during the Paleoproterozoic assembly of Columbia. *Earth Planet. Sci. Lett.*, **579**, 117342. doi: 10.1016/j.epsl.2021.117342

Zhang, P., Miller, M.S., 2021. Seismic Imaging of the Subducted Australian Continental Margin Beneath Timor and the Banda Arc Collision Zone. *Geophys. Res. Lett.*, **48**(4), e2020GL089632. doi: 10.1029/2020GL089632.